



# Journal of Applied and Computational Mechanics



## Research Paper

# Effect of Magnetic Field on Viscous Flow through Composite Porous Channel using Boundary Element Method

Vishal Chhabra<sup>id</sup>, Chandra Shekhar Nishad<sup>id</sup>, Manoj Sahni<sup>id</sup>

School of Technology, Department of Mathematics, Pandit Deendayal Energy University, Gandhinagar, Gujarat 382426, India  
Email: Vishalchhabra854@gmail.com (V.C.); Chandra.Nishad@sot.pdpu.ac.in (C.S.N.); Manoj.Sahni@sot.pdpu.ac.in (M.S.)

Received February 13 2023; Revised April 06 2023; Accepted for publication April 15 2023.

Corresponding author: C.S. Nishad (Chandra.Nishad@sot.pdpu.ac.in)

© 2023 Published by Shahid Chamran University of Ahvaz

**Abstract.** In this paper, we investigate the effect of magnetic field on two-dimensional flow of a viscous, incompressible fluid through composite porous channel using non-primitive boundary element method (BEM). We consider a rectangular channel consisting of two packings that are filled with fully saturated porous medium. It is assumed that both the porous regions are homogenous and isotropic with different permeabilities. Brinkman equation governs the fluid flow through porous media. We analyze the effect of Hartman number, stress-jump coefficient, Darcy number, thickness parameter, electrical conductivity ratio, and viscosity ratio on fluid mechanics. We present the effect of stress-jump coefficients on the interfacial velocity of the fluid against the thickness parameter and observe that the interfacial velocity increases with increasing stress-jump coefficients. We notice that for a fixed value of thickness parameter, the magnitude of vorticity (at lower and upper walls) increases with increasing Darcy number. Moreover, we observe that the magnitude of vorticity at the lower wall decreases and increases at the upper wall with increasing thickness parameter. We compute the Brinkman layer thickness near the interface of the composite porous channel in terms of several flow parameters and observe that the Brinkman layer thickness is strongly depend on the Hartman number, Darcy number, viscosity ratios, and stress-jump coefficient, respectively.

**Keywords:** Boundary element method, Brinkman equation, Hartmann number, Stress-jump condition, Brinkman layer.

## 1. Introduction

Fluid flow problems have numerous applications in climatology, fluid control system, and oceanography. Also, it has widespread environmental and industrial applications like groundwater hydrology, extraction of ceramics and industrial fluids from reservoirs, composite material processing, solidifications of casting and overland flow during rainfall, etc. Which encourages several researchers to study fluid dynamics [1– 4].

The study of viscous flow through the composite porous channel attracts many researchers due to its involvement in oil extraction processes from the earth, underground water recovery and some biological processes, etc. [5]. Allan and Hamdan [6] studied fluid mechanics in between two porous regions consisting in a composite channel. Forchheimer and Brinkman equations were used by them to govern the fluid flow from the first and second porous regions, respectively. Fluid flow from the composite porous channel has extensive applications in the fields of chemical and agricultural engineering, etc. Turkyilmazoglu [7] presented an exact solution for the velocity, pressure, and shear stress of the viscous flow over the porous rotating disk. The solutions are presented in terms of dimensionless parameters. The findings evince that the velocity and shear stress of the fluid augments as a function of the rising porosity of the porous rotating disk. Additionally, velocity and shear stress are found to increase the Reynolds number and decrease with the increasing Prandtl number. Later, the direct method was devised by [8] to investigate the non-linear porous fin problem, associated with two parameters namely the material's porosity and Biot number. Also, obtained the temperature profile at the tip of the fin as well as the corresponding heat transfer rate. Yadav and Verma [9] analyzed the flow behavior of two immiscible fluids through an inclined porous channel, assuming both porous media had distinct permeabilities. Also, the comprehensive analysis of multiple flow variables is elucidated.

The Brinkman equation is used instead of Darcy's law when fluid flowing through porous medium is viscous in nature. Due to the appearance of spatial derivatives of the velocity, we need a boundary condition at the interface called stress-jump boundary condition, which is the very first time presented by Ochoa-Tapia and Whitaker [10, 11]. Using this condition, they resolve the problem given by Neale and Nader [12]. Ahmadi et al. [13] used primitive approach in the boundary element method to analyze fluid flow specifically at the interface between two porous packings of the channel. The Brinkman equation was used by them to govern the flow. Also, they implemented the jump condition for shear stress at the interface of both porous packings of the channel. Subsequently, reveals stress-jump coefficient dependency on the porous medium structure. Turkyilmazoglu [14] analyze the dynamics of velocity slip and the emergence of entropy in thermal transport across a metallic porous channel and



found that velocity slip can significantly affect the heat transfer and entropy generation in the channel, and increase the porosity of the material can enhance the heat transfer while reducing the entropy generation.

Nowadays, the importance of magnetic field has increased significantly as a result of their many important applications in medical, industrial fields, and bioengineering fields, such as hyperthermia, treatment of wounds, power generators, catalytic reactions, aerodynamic heating, distillation towers, electrostatic precipitation, etc. [15]. Aydin and Selvitopi [16] used BEM and finite element method (FEM) coupling approach to analyze the MHD flow through an unbounded external domain. They considered an inclined magnetic field and discretized the domain and its boundary with the help of both the BEM and FEM coupling approaches. Also, they have shown the contour diagram for velocity and induced current for distinct combination of Hartman number, and other flow parameters. Bali and Awasthi [17] analyzed the influence of an applied magnetic field on blood flow through a stenotic artery. They considered the viscosity of blood as radial coordinate dependent. Verma and Datta [18] analyzed the impact of an applied transverse magnetic field on electrically conducting, viscous, and incompressible fluid. Also, they analyzed the behavior of fluid mechanics by varying viscosity graphically. Tiwari et al. [19] presented the variation of hydrodynamic permeability on fluid mechanics for different values of the Hartman number. Manyonge et al. [20] extended the work of Verma and Datta [18], by taking flow through two infinite parallel plates. Also, they studied the impact of an inclined magnetic field on fluid velocity. Ansari and Deo [21] analyzed the dependency of velocity profile on transport parameters in the existence of the magnetic field, but not included several parameters like jump in shear stress, fluids having different permeability, and interfacial velocity, which can affect the velocity profile along with Hartman number. Wahid et al. [22] utilized an exact analytical method to obtain the boundary layer flow and heat transfer of Casson fluid confined by a stretching surface with the presence of viscous dissipation. They observed that the skin friction coefficient increases with the increase in magnetohydrodynamic (MHD) parameter and decreases with the decrease in velocity slip. Also, the presence of velocity slip and, other parameters are enhancing the temperature profile and as these parameters increase, there is a decrement in the heat transfer coefficient.

The impact of magnetic field on micropolar fluid passing through non-permeable porous membranes was investigated by Yadav et al. [23]. They presented the impact of flow parameters including Hartman number, etc. on the fluid mechanics. Later, Jaiswal and Yadav [24] analyzed the influence of an applied magnetic field on blood flowing through porous arteries. They have taken different permeabilities of both phases. They conclude that flow velocity in the core region is inversely proportional to the intensity of the magnetic field. After that, the influence of the magnetic field on Jeffrey fluid passing through two-phase permeable medium was observed by Ge-JiLe et al. [15]. They also observed that there is a decrement in velocity as the Hartman number increases, and there is a rise in flow due to Darcy's number. Yadav and Verma [25] extended the work of [9] by assuming different permeabilities of both porous packings consisting of a channel. They observed the impact of several transport parameters like viscosity ratio, permeability, etc. on fluid mechanics. A numerical technique called stabilized FEM was utilized by [26] to solve coupled convection-diffusion type MHD equations. Contour diagrams depicting the velocity field and magnetic induction were presented for distinct values of Hartman number and angles of MHD flow in a T-shaped domain. Selvitopi [27] employed both the finite difference method and the Galerkin FEM to inspect the complex dynamics of damped wave-type MHD flow. The numerical exploration was conducted with the utmost precision in a substantially elongated rectangular channel, pervaded by a time-varying oblique magnetic field, to uncover the intricacies of the underlying physics. Upon close examination, it was duly noted that the emergence of the Hartman layer is the direct consequence of elevated Hartman numbers, impeccably aligning with the inherent characteristics of the MHD flow.

In literature, thickness and permeability of both the porous regions in a rectangular channel have taken fixed but in the present study, we consider the variation of thickness parameter and permeability in both the porous regions. In this manner, we can adjust the thickness and permeability of both porous packings of the channel according to our physical problem. We have applied a jump in shear stress at the interface of both porous mediums, which is not much explored in the literature.

Although the present problem can be solved analytically, when the geometry is irregular and/or boundary conditions are non-linear, an analytical solution is not possible. In that case, we need a reliable numerical technique to solve the problem. In literature, several numerical techniques have been discussed. We have observed from the literature that for irregular geometry, Boundary Element Method (BEM) has an advantage over any other numerical method. BEM is based on the integral equation method. Recently, Nishad et al. [28] developed the boundary element technique based on non-primitive variables approach for modelling the 2D flow of a viscous incompressible fluid through a rectangular channel consisting of two porous packings. In the present work, the boundary element technique based on non-primitive variables approach is utilized to analyze the influence of magnetic field on viscous fluid passing through a composite porous channel.

The layout of the paper is arranged as follows: Section 2, describes the mathematical modelling of the physical problem to investigate the effect of transverse magnetic field on Brinkman flow through a 2D composite porous channel. To solve the mathematical equation, we transform the differential equation to its equivalent form of boundary integral equations. Section 3, presents the impact of several transport parameters on the velocity of the fluid to analyze the flow mechanics. A brief overview of the current investigation is provided in Section 4.

## 2. Mathematical Modelling of the Physical Problem

### 2.1 Two-dimensional composite porous channel with an applied transverse magnetic field: Governing equations

The motivation for analyzing the impact of the magnetic field on the physics of fluid through a rectangular channel having two porous packings arises because of widespread industrial, environmental, and medical applications such as the process of extracting oils, polymer technology, control of aerodynamical boundary layer, filtration of underground different fluids flowing together, treatment of cancer and cardiovascular diseases, etc. In this study, we consider Brinkman flow through two-dimensional rectangular porous channel consisting of two porous packings having distinct permeability (refer to Fig. 1).

We consider that the porous media is homogenous and isotropic. The porous regions above and below the interface are denoted by  $\Omega^{(1)}$  and  $\Omega^{(2)}$ , respectively. A magnetic field ( $\vec{B}$ ) with uniform intensity is applied in the orthogonal direction to the flow. The viscous fluid passing through a channel consisting of two packings filled with the fully saturated porous medium in the presence of magnetic field is governed by the Brinkman equation which includes the term which represents Lorentz force, combined with the continuity equation, which is as follows ([21, 29]):

$$\tilde{\mu}_e \nabla^2 \vec{v}_i - \frac{\tilde{\mu}_i}{k_i} \vec{v}_i + \vec{j} \times \vec{B} = \vec{\nabla} p_i \quad (1)$$

$$\vec{\nabla} \cdot \vec{v}_i = 0 \quad (2)$$



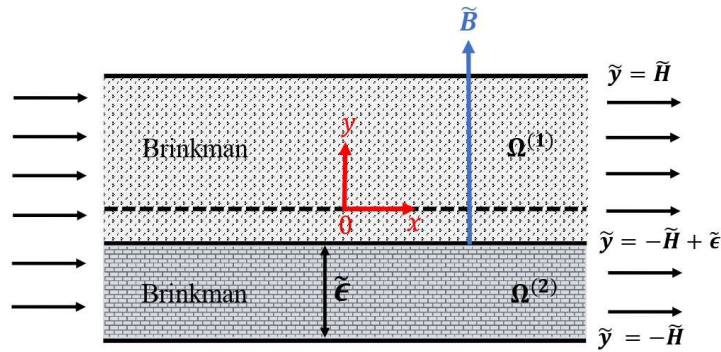


Fig. 1. Schematic of the physical problem.

where  $\tilde{\mathbf{v}}_i = (\tilde{u}_i, \tilde{v}_i)$  represents the velocity vector in the regions  $\Omega^{(i)} (i=1,2)$ . Here,  $\tilde{k}_i, \tilde{p}_i, \tilde{\mu}_e$  and  $\tilde{\mu}_i$  are permeability, hydrodynamic pressure, effective viscosity of the porous matrix, and fluid viscosity in  $\Omega^{(i)} (i=1,2)$  respectively. In the absence of an external electric field and considering the insignificant effect of induced current, the electric current density  $\tilde{\mathbf{j}} = \tilde{\sigma}(\tilde{\mathbf{v}} \times \tilde{\mathbf{B}})$ , where  $\tilde{\sigma}$  denotes the electrical conductivity of the fluid. Hence, it is concluded that Lorentz force and velocity are collinear and opposite in the directions, hence  $\tilde{\mathbf{F}} = \tilde{\mathbf{j}} \times \tilde{\mathbf{B}}$  implies  $\tilde{\mathbf{F}} = -\tilde{\sigma}\tilde{B}_0^2\tilde{\mathbf{v}}$ , where  $\tilde{B}_0 = |\tilde{\mathbf{B}}|$ . Magnetic induction equation is eliminated here, due to the assumption that the magnetic Reynolds number  $R_m$  is small. When  $R_m \ll 1$ , the magnetic field is said to be frozen into the fluid, meaning that the fluid moves with the magnetic field lines. This assumption allows us to neglect the inertial effects of the magnetic field on the fluid and reduces the magnetic induction equation to a simple diffusion equation. We assume  $\tilde{\mu}_e = \tilde{\mu}_i$  for both regions. Therefore, Eqs. (1) and (2) become:

$$\tilde{\nabla}^2 \tilde{\mathbf{v}}_i - \frac{\tilde{\mathbf{v}}_i}{\tilde{k}_i} - \frac{\tilde{\sigma}_i \tilde{B}_0^2 \tilde{\mathbf{v}}_i}{\tilde{\mu}_i} = \frac{\tilde{\nabla} \tilde{p}_i}{\tilde{\mu}_i} \quad (3)$$

$$\tilde{\nabla} \cdot \tilde{\mathbf{v}}_i = 0 \quad (4)$$

## 2.2 Transformation of governing equations into dimensionless form

Introducing the dimensionless variables as follows:

$$\mathbf{v}_i = \frac{\tilde{\mathbf{v}}_i}{\tilde{U}}, x = \frac{\tilde{x}}{\tilde{H}}, y = \frac{\tilde{y}}{\tilde{H}}, p_i = \frac{\tilde{p}_i}{\tilde{p}_0}, \tilde{p}_0 = \frac{\tilde{\mu}_1 \tilde{U}}{\tilde{H}}, \alpha = \frac{\tilde{\mu}_1}{\tilde{\mu}_2}, \gamma = \frac{\tilde{\sigma}_1}{\tilde{\sigma}_2}, \epsilon = \frac{\tilde{\epsilon}}{\tilde{H}}, \tilde{\nabla} = \frac{\tilde{\nabla}}{\tilde{H}} \quad (5)$$

where  $\tilde{H}, \tilde{U}$  represents the characteristic length and velocity respectively. The dimensionless form of momentum and continuity equations for the region  $\Omega^{(1)}$  and  $\Omega^{(2)}$  are given as follows:

$$\nabla^2 \mathbf{v}_1 - t_1^2 \mathbf{v}_1 = \nabla p_1, \quad \nabla \cdot \mathbf{v}_1 = 0 \quad (6)$$

$$\nabla^2 \mathbf{v}_2 - t_2^2 \mathbf{v}_2 = \alpha \nabla p_2, \quad \nabla \cdot \mathbf{v}_2 = 0 \quad (7)$$

where  $t_i^2 = (n_i^2 + M_i^2)$ ,  $n_i^2 = \tilde{H}^2 / \tilde{k}_i = 1 / Da_i$  (here,  $Da_i$  are Darcy numbers, i.e.,  $Da_i = \tilde{k}_i / \tilde{H}^2$  [13]) for  $i=1,2$ ,  $M_1 = M_2 \sqrt{\alpha / \gamma}$  and  $M_1 = \sqrt{\tilde{\sigma}_1 \tilde{B}_0^2 \tilde{H}^2 / \tilde{\mu}_1}$ . Here,  $M_1, M_2$  are Hartman numbers in  $\Omega^{(1)}$  and  $\Omega^{(2)}$ , respectively.

## 2.3 Non-dimensional boundary conditions

1. No-slip condition at upper plate  $y = 1$ :

$$u_1 = 0, v_1 = 0. \quad (8)$$

2. No-slip condition at lower plate  $y = -1$ :

$$u_2 = 0, v_2 = 0. \quad (9)$$

3. At the upstream:

$$u_i = \frac{3}{2}(1 - y^2), v_i = 0 \text{ for } i = 1, 2. \quad (10)$$

4. At the downstream:

$$\frac{\partial u_i}{\partial x} = 0, \frac{\partial v_i}{\partial x} = 0 \text{ for } i = 1, 2. \quad (11)$$

5. At the porous-porous interface ( $y = -1 + \epsilon$ ):

5.1. Velocity continuity:

$$u_1 = u_2, v_1 = v_2. \quad (12)$$



## 5.2. Jump in shear stress [13]:

$$\mu_1 \frac{\partial u_1}{\partial y} - \mu_2 \frac{\partial u_2}{\partial y} = \mu_1 \left( \frac{\beta_1}{\sqrt{Da_1}} - \frac{\beta_2}{\sqrt{Da_2}} \right) u_1. \quad (13)$$

where  $\beta_1, \beta_2$  are stress-jump coefficients.

## 5.3. Normal stress continuity ([13, 32]):

$$-P_1 + 2 \frac{\partial v_1}{\partial y} = -P_2 + 2 \frac{\partial v_2}{\partial y}. \quad (14)$$

## 2.4 Reduction of Governing equations in terms of non-primitive variables

The velocity field can be written in terms of stream function ([30]) with the help of the continuity equation:

$$u_i = \frac{\partial \Psi^{(i)}}{\partial y}, \quad v_i = -\frac{\partial \Psi^{(i)}}{\partial x}, \quad (i = 1, 2). \quad (15)$$

To reduce Eqs. (6) and (7) into boundary value problem, we substitute  $\mathbf{v}_i = (u_i, v_i)$  ( $i = 1, 2$ ) in Eqs. (6) and (7), we get Eqs. (16) and (17), respectively:

$$\nabla^2 \mathbf{v}_1 - t_1^2 \mathbf{v}_1 = \nabla p_1 \Rightarrow \nabla^2 (u_1, v_1) - t_1^2 (u_1, v_1) = \left( \frac{\partial}{\partial x}, \frac{\partial}{\partial y} \right) p_1 \Rightarrow \nabla^2 u_1 - t_1^2 u_1 = \frac{\partial p_1}{\partial x}, \quad \nabla^2 v_1 - t_1^2 v_1 = \frac{\partial p_1}{\partial y}. \quad (16)$$

$$\nabla^2 \mathbf{v}_2 - t_2^2 \mathbf{v}_2 = \alpha \nabla p_2 \Rightarrow \nabla^2 (u_2, v_2) - t_2^2 (u_2, v_2) = \left( \frac{\partial}{\partial x}, \frac{\partial}{\partial y} \right) \alpha p_2, \Rightarrow \nabla^2 u_2 - t_2^2 u_2 = \alpha \frac{\partial p_2}{\partial x}, \quad \nabla^2 v_2 - t_2^2 v_2 = \alpha \frac{\partial p_2}{\partial y}. \quad (17)$$

Further, Eq. (16) can be solved as follows:

$$\Rightarrow \frac{\partial}{\partial y} \left( \nabla^2 u_1 - t_1^2 u_1 = \frac{\partial p_1}{\partial x} \right) - \frac{\partial}{\partial x} \left( \nabla^2 v_1 - t_1^2 v_1 = \frac{\partial p_1}{\partial y} \right) \Rightarrow \nabla^2 \left( \frac{\partial u_1}{\partial y} - \frac{\partial v_1}{\partial x} \right) - t_1^2 \left( \frac{\partial u_1}{\partial y} - \frac{\partial v_1}{\partial x} \right) = \frac{\partial}{\partial y} \left( \frac{\partial p_1}{\partial x} \right) - \frac{\partial}{\partial x} \left( \frac{\partial p_1}{\partial y} \right), \quad (18)$$

$$\Rightarrow \nabla^2 \left[ \frac{\partial}{\partial y} \left( \frac{\partial \Psi^{(1)}}{\partial y} \right) - \frac{\partial}{\partial x} \left( -\frac{\partial \Psi^{(1)}}{\partial x} \right) \right] - t_1^2 \left[ \frac{\partial}{\partial y} \left( \frac{\partial \Psi^{(1)}}{\partial y} \right) - \frac{\partial}{\partial x} \left( -\frac{\partial \Psi^{(1)}}{\partial x} \right) \right] = 0 \Rightarrow \nabla^2 (\nabla^2 \Psi^{(1)}) - t_1^2 (\nabla^2 \Psi^{(1)}) = 0 \Rightarrow \nabla^2 (\nabla^2 - t_1^2) \Psi^{(1)} = 0. \quad (19)$$

Similarly, Eq. (17) can be solved as:

$$\Rightarrow \frac{\partial}{\partial y} \left( \nabla^2 u_2 - t_2^2 u_2 = \alpha \frac{\partial p_2}{\partial x} \right) - \frac{\partial}{\partial x} \left( \nabla^2 v_2 - t_2^2 v_2 = \alpha \frac{\partial p_2}{\partial y} \right) \Rightarrow \nabla^2 \left( \frac{\partial u_2}{\partial y} - \frac{\partial v_2}{\partial x} \right) - t_2^2 \left( \frac{\partial u_2}{\partial y} - \frac{\partial v_2}{\partial x} \right) = \alpha \left[ \frac{\partial}{\partial y} \left( \frac{\partial p_2}{\partial x} \right) - \frac{\partial}{\partial x} \left( \frac{\partial p_2}{\partial y} \right) \right], \quad (20)$$

$$\Rightarrow \nabla^2 \left[ \frac{\partial}{\partial y} \left( \frac{\partial \Psi^{(2)}}{\partial y} \right) - \frac{\partial}{\partial x} \left( -\frac{\partial \Psi^{(2)}}{\partial x} \right) \right] - t_2^2 \left[ \frac{\partial}{\partial y} \left( \frac{\partial \Psi^{(2)}}{\partial y} \right) - \frac{\partial}{\partial x} \left( -\frac{\partial \Psi^{(2)}}{\partial x} \right) \right] = 0 \Rightarrow \nabla^2 (\nabla^2 \Psi^{(2)}) - t_2^2 (\nabla^2 \Psi^{(2)}) = 0 \Rightarrow \nabla^2 (\nabla^2 - t_2^2) \Psi^{(2)} = 0. \quad (21)$$

This follows from the Eqs. (19) and (21) that:

$$\nabla^2 (\nabla^2 - t_i^2) \Psi^{(i)} = 0, \quad (22)$$

where  $t_i^2 = (n_i^2 + M_i^2)$ , ( $i = 1, 2$ ).

Nishad et al. [31] developed a non-primitive BEM to solve the 2D Brinkman equation. We introduce the vorticity variable  $\omega^{(i)}$ , by using Eq. (15):

$$\omega^{(i)} = \nabla \times \mathbf{v}_i = \nabla \times (u_i, v_i) = \left( \frac{\partial v_i}{\partial x} - \frac{\partial u_i}{\partial y} \right) = \left[ \frac{\partial}{\partial x} \left( -\frac{\partial \Psi^{(i)}}{\partial x} \right) - \frac{\partial}{\partial y} \left( \frac{\partial \Psi^{(i)}}{\partial y} \right) \right] = - \left( \frac{\partial^2 \Psi^{(i)}}{\partial x^2} + \frac{\partial^2 \Psi^{(i)}}{\partial y^2} \right) = -\nabla^2 \Psi^{(i)}. \quad (23)$$

To solve Eq. (22), we reduce Eq. (22) into a coupled system of Poisson (Eq. (23)) and modified Helmholtz equations (by substituting Eq. (23) into Eq. (22)), which are as follows:

$$\nabla^2 \Psi^{(i)} = -\omega^{(i)}, \quad (24)$$

$$(\nabla^2 - t_i^2) \omega^{(i)} = 0. \quad (25)$$

## 2.5 Reduction of boundary conditions in terms of non-primitive variables

1. No-slip condition at upper plate  $y = 1$ :

$$\Psi^{(1)} = 1, \quad \frac{\partial \Psi^{(1)}}{\partial y} = 0. \quad (26)$$

2. No-slip condition at lower plate  $y = -1$ :





$$\psi^{(2)} = -1, \frac{\partial \psi^{(2)}}{\partial y} = 0. \quad (27)$$

3. At the upstream:

$$\psi^{(i)} = \frac{3}{2} \left( y - \frac{y^3}{3} \right), \omega^{(i)} = 3y, \text{ for } i = 1, 2. \quad (28)$$

4. At the downstream:

$$\frac{\partial \psi^{(i)}}{\partial x} = 0, \frac{\partial \omega^{(i)}}{\partial x} = 0, \text{ for } i = 1, 2. \quad (29)$$

5. At the porous-porous interface ( $y = -1 + \epsilon$ ):

5.1. Velocity continuity

$$\psi^{(1)} = \psi^{(2)}, \frac{\partial \psi^{(1)}}{\partial y} = \frac{\partial \psi^{(2)}}{\partial y} \quad (30)$$

5.2. Jump in shear stress:

$$\mu_1 \omega^{(1)} = - \left[ \mu_2 \omega^{(2)} + \mu_1 \left( \frac{\beta_1}{\sqrt{Da_1}} - \frac{\beta_2}{\sqrt{Da_2}} \right) \frac{\partial \psi^{(1)}}{\partial y} \right]. \quad (31)$$

To establish the above relationship, we employ a step-by-step approach. Initially, we utilize Eq. (12). Subsequently, we use Eq. (15). Finally, we make use of the relation, as stated by Eq. (24). By following these steps, Eq. (13) is simplified and ultimately reduced to Eq. (31).

5.3. Normal stress continuity:

$$\frac{\partial \omega^{(1)}}{\partial y} + t_1^2 \frac{\partial \psi^{(1)}}{\partial y} = - \frac{1}{\alpha} \left( t_2^2 \frac{\partial \psi^{(2)}}{\partial y} - \frac{\partial \omega^{(2)}}{\partial y} \right), \quad (32)$$

where  $t_i^2 = (n_i^2 + M_i^2)$ , ( $i = 1, 2$ ). and  $\alpha = \mu_1 / \mu_2$ .

## 2.6 Non-primitive boundary element method for Brinkman-Brinkman system

To ensure a clear understanding of the numerical solution procedure, it is necessary to discuss the algorithm in detail before moving forward. The following steps are as follows:

### Algorithm 1. Algorithm of the Numerical Solution Procedure

Step 1.	Formulation of boundary value problem (BVP) by defining the relevant physics and mathematics governing the problem at hand.
Step 2.	Computation of the free space Green's function or fundamental solution.
Step 3.	Utilization of Green's second identity, which relates the behavior of a system inside a closed boundary to the sources and sinks of the system outside that boundary.
Step 4.	Derivation of boundary integral formulation (BIF), which transforms the original BVP into a set of equations that can be solved using only boundary data. This is where the BEM comes into play, as it is used for boundary information.
Step 5.	Discretization of the boundary integral equations using suitable elements (BEM), allowing for an efficient and accurate numerical solution.
Step 6.	Evaluation of boundary integrals (also called influence coefficients), representing the sensitivity of the boundary values to variations in the sources.
Step 7.	Solution corresponding to the system of linear equations to get the unknown boundary data.
Step 8.	Evaluation of solution at any point inside the given domain.

Let  $p(X_0, Y_0)$ , and  $q(X, Y)$  be the field point and integration point, respectively. Here,  $p \in \Omega \cup \Lambda$ , and  $q \in \Lambda$ , where  $\Omega = \Omega^{(1)} \cup \Omega^{(2)}$ , and  $\Lambda = \Lambda^{(1)} \cup \Lambda^{(2)}$ . We assume that the outer boundaries of the regions  $\Omega^{(1)}$ , and  $\Omega^{(2)}$  are denoted by  $\Lambda^{(1)}$  and  $\Lambda^{(2)}$ , respectively and  $\Lambda^{(12)}$  denote the interface region where  $\Lambda^{(1)*} = \Lambda^{(1)} \cup \Lambda^{(12)}$ , and  $\Lambda^{(2)*} = \Lambda^{(2)} \cup \Lambda^{(12)}$ , (refer to Fig. 2). Let  $G^L, G^{MH}$  and  $G^C$  represents free space Green's function with respect to Laplacian, modified Helmholtz, and composite operator given by  $G_i^L = \ln \hat{r} / 2\pi$ ,  $G_i^{MH} = -K_0(t_i \hat{r}) / 2\pi$ , and  $G_i^C = (G_i^{MH} - G_i^L) / t_i^2$ , ( $i = 1, 2$ ) where  $K_0$  represents the modified Bessel function of zeroth order of second kind and  $\hat{r} = |p - q|$ .

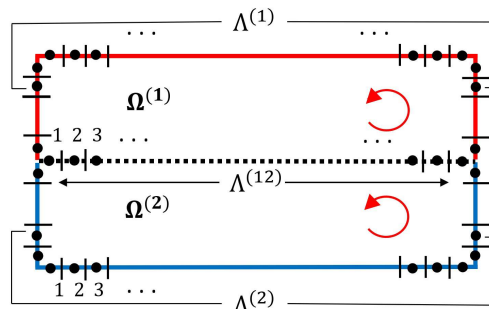


Fig. 2. Discretization of the boundary of the computational domain [28].



Applying Green's second identity to Eqs. (24) and (7) together with the fundamental solution, we obtain boundary integral equations (please refer to Appendix C) at any field point  $p$ :

$$c(p)\psi^{(i)}(p) = \int_{\Lambda^{(i)}} \left( \psi^{(i)}(q) \frac{\partial G_i^L(p, q)}{\partial n_q} - G_i^L(p, q) \frac{\partial \psi^{(i)}(q)}{\partial n_q} \right) ds(q) - \int_{\Lambda^{(i)}} \left( \omega^{(i)}(q) \frac{\partial G_i^C(p, q)}{\partial n_q} - G_i^C(p, q) \frac{\partial \omega^{(i)}(q)}{\partial n_q} \right) ds(q) \quad (33)$$

$$c(p)\omega^{(i)}(p) = \int_{\Lambda^{(i)}} \left( \omega^{(i)}(q) \frac{\partial G_i^{MH}(p, q)}{\partial n_q} - G_i^{MH}(p, q) \frac{\partial \omega^{(i)}(q)}{\partial n_q} \right) ds(q) \quad (34)$$

where free term coefficient  $c(p)$  is defined as:

$$c(p) = \begin{cases} 1, & p \in \Omega \\ \frac{1}{2}, & p \in \Lambda \\ 0, & p \notin \Omega \cup \Lambda \end{cases} \quad (35)$$

Here, Eqs. (33) and (34) involves weakly singular (free space Green's function) and strongly singular (normal derivatives of free space Green's function) kernels inside the integrals. In this case, one has to handle these singularities very carefully. Also, most of the time, the boundary of the computational domain is irregular in shape. In this scenario, analytical evaluation of the integrals is not possible. Therefore, numerical treatment is needed at the boundary. In order to compute the integrals in Eqs. (33) and (34), we approximate the boundary by straight line segments and assumed boundary quantity constant. Further, we discretize the boundary  $\Lambda^{(1)}$ ,  $\Lambda^{(2)}$ ,  $\Lambda^{(12)}$ ,  $\Lambda^{(1)}$ , and  $\Lambda^{(2)}$  into  $N^{(1)}$ ,  $N^{(2)}$ ,  $N^{(12)}$ ,  $N^{(1)}$ , and  $N^{(2)}$  constant elements respectively, which is the simplest constant element in the positive orientation sense, where  $N^{(1)} = N^{(1)} + N^{(12)}$ , and  $N^{(2)} = N^{(2)} + N^{(12)}$  (refer to Fig. 2). The boundary quantities  $\psi$ ,  $\partial\psi/\partial n$ ,  $\omega$ , and  $\partial\omega/\partial n$  are approximated by piece-wise constant functions  $\psi_j$ ,  $\partial\psi_j/\partial n$ ,  $\omega_j$ , and  $\partial\omega_j/\partial n$  over each element  $\Lambda^{(i)}$ ,  $j = 1, 2, \dots, N^{(i)}$ , ( $i = 1, 2$ ).

Applying the corresponding discretized forms of Eqs. (33) and (34) at the mid-point  $p \equiv q_l$ ,  $l = 1, 2, \dots, N^{(i)}$  of each element (this process is called collocation), we obtain:

$$c_i \psi^{(i)} = \sum_{j=1}^{N^{(i)}} \left[ \psi_j^{(i)} \int_{q \in \Lambda_j^{(i)}} \frac{\partial G_i^L(q_l, q)}{\partial n_q} ds(q) - \frac{\partial \psi_j^{(i)}}{\partial n_q} \int_{q \in \Lambda_j^{(i)}} G_i^L(q_l, q) ds(q) - \omega_j^{(i)} \int_{q \in \Lambda_j^{(i)}} \frac{\partial G_i^C(q_l, q)}{\partial n_q} ds(q) + \frac{\partial \omega_j^{(i)}}{\partial n_q} \int_{q \in \Lambda_j^{(i)}} G_i^C(q_l, q) ds(q) \right] \quad (36)$$

$$c_i \omega^{(i)} = \sum_{j=1}^{N^{(i)}} \left[ \omega_j^{(i)} \int_{q \in \Lambda_j^{(i)}} \frac{\partial G_i^{MH}(q_l, q)}{\partial n_q} ds(q) - \frac{\partial \omega_j^{(i)}}{\partial n_q} \int_{q \in \Lambda_j^{(i)}} G_i^{MH}(q_l, q) ds(q) \right] \quad (37)$$

The equivalent form of Eqs. (36) and (37) is given by:

$$A_{ij}^{(i)} \psi^{(i)} + B_{ij}^{(i)} \frac{\partial \psi^{(i)}}{\partial n} + C_{ij}^{(i)} \omega^{(i)} + D_{ij}^{(i)} \frac{\partial \omega^{(i)}}{\partial n} = 0 \quad (38)$$

$$E_{ij}^{(i)} \omega^{(i)} + F_{ij}^{(i)} \frac{\partial \omega^{(i)}}{\partial n} = 0 \quad (39)$$

where the influence coefficients are given by:

$$A_{ij}^{(i)} = \int_{q \in \Lambda_j^{(i)}} \frac{\partial G_i^L(q_l, q)}{\partial n_q} ds(q) - c_j \delta_{ij}, \quad B_{ij}^{(i)} = - \int_{q \in \Lambda_j^{(i)}} G_i^L(q_l, q) ds(q) \quad (40)$$

$$C_{ij}^{(i)} = - \int_{q \in \Lambda_j^{(i)}} \frac{\partial G_i^C(q_l, q)}{\partial n_q} ds(q), \quad D_{ij}^{(i)} = \int_{q \in \Lambda_j^{(i)}} G_i^C(q_l, q) ds(q) \quad (41)$$

$$E_{ij}^{(i)} = \int_{q \in \Lambda_j^{(i)}} \frac{\partial G_i^{MH}(q_l, q)}{\partial n_q} ds(q) - c_j \delta_{ij}, \quad F_{ij}^{(i)} = - \int_{q \in \Lambda_j^{(i)}} G_i^{MH}(q_l, q) ds(q) \quad (42)$$

where  $\delta_{ij}$  represents the Kronecker delta function. We denote  $(A^{(i)})_{ij} = A_{ij}^{(i)}$  and  $\psi^{(i)} = (\psi^{(i)}, \psi^{(i)}, \dots, \psi_{N^{(i)}}^{(i)})$  etc. To obtain the information of the unknown boundary data, we solve Eqs. (38) and (39), with the help of Eqs. (26)-(32). The systems stated by Eqs. (38) and (39) have more number  $(2N^{(1)} + 2N^{(2)} + 8N^{(12)})$  of unknowns than the number  $(2N^{(1)} + 2N^{(2)} + 4N^{(12)})$  of equations, which results in an inconsistent system. In order to make the system solvable, we apply interfacial boundary conditions given by Eqs. (30)-(32). In this manner, the resultant system of linear algebraic equations has an equal number of equations and unknowns. Once we know all the boundary data, we get  $\psi^{(i)}, \omega^{(i)}$ , ( $i = 1, 2$ ) at general field point inside the computational domain. In BEM simulation, to discretize the boundary of each domain, we have considered 220 straight-line elements. This follows that 220 number of nodes for each domain, as the node is present in the mid of the straight line. We cross-verified that there is no significant change in computed values if we increase the boundary elements. We have used 2500 (i.e.,  $50 \times 50$ ) solution points ( $N_s$ ) inside each domain.



To execute the numerical implementation, MATLAB®(R2014b) has been utilized. To execute BEM code, PC having the properties Intel(R) Core (TM) i5-2400 CPU@ 3.10 GHz processor has been used. The estimated computational time to run the BEM code in MATLAB is 23.666407 seconds.

## 2.7 Evaluation of singular boundary integrals

When  $l \neq j$ , then integrals are free from any singularity. As a result, the numerical Gauss quadrature method can be utilized to evaluate regular these integrals. In case, when  $l = j$ , the vector  $\mathbf{r}$  lies on the  $j^{\text{th}}$  element, where  $\hat{r}$  is the magnitude of  $\mathbf{r}$  i.e.,  $\hat{r} = |\mathbf{p} - \mathbf{q}| = |\mathbf{r}|$  is consistently orthogonal to the orthogonal vector  $\mathbf{n}$ , then integrals stated by Eqs. (40)-(42) become singular. In situations involving constant elements, integrals having singularity can be deduced via analytical computation. The influence coefficients  $A_{jj}$  and  $B_{jj}$  are obtained and presented as follows (please refer to [33, 34]):

$$A_{jj} = -c_j, B_{jj} = -\frac{\tilde{l}_j}{2\pi} \left[ \ln \left( \frac{\tilde{l}_j}{2} \right) - 1 \right], \quad (43)$$

where  $\tilde{l}_j$  denotes the length of the  $j^{\text{th}}$  element. To solve  $C_{jj}$ ,  $D_{jj}$ ,  $E_{jj}$  and  $F_{jj}$ , we proceed with the methodology utilized by Nishad et al. [33] and obtained the expressions for these singular integrals analytically. The fundamental solutions namely,  $G_i^L$ ,  $G_i^{MH}$  and  $G_i^C$  and their normal derivatives are as follows:

$$G_i^L = \frac{1}{2\pi} \ln \hat{r}, \quad \frac{\partial G_i^L}{\partial \mathbf{n}} = \frac{1}{2\pi \hat{r}} \frac{\partial \hat{r}}{\partial \mathbf{n}} = \frac{\mathbf{r} \cdot \mathbf{n}}{2\pi \hat{r}^2}, \quad (44)$$

$$G_i^{MH} = -\frac{1}{2\pi} K_0(t_i \hat{r}), \quad \frac{\partial G_i^{MH}}{\partial \mathbf{n}} = \frac{t_i}{2\pi} K_1(t_i \hat{r}) \frac{\partial \hat{r}}{\partial \mathbf{n}} = \frac{t_i}{2\pi} K_1(t_i \hat{r}) \frac{\mathbf{r} \cdot \mathbf{n}}{\hat{r}}, \quad (i = 1, 2). \quad (45)$$

$$G_i^C = \frac{1}{t_i^2} (G_i^{MH} - G_i^L), \quad \frac{\partial G_i^C}{\partial \mathbf{n}} = \frac{1}{t_i^2} \left( \frac{\partial G_i^{MH}}{\partial \mathbf{n}} - \frac{\partial G_i^L}{\partial \mathbf{n}} \right), \quad (i = 1, 2). \quad (46)$$

As  $\hat{r} \rightarrow 0$ , i.e., the asymptotic behavior of  $K_0(t_i \hat{r})$  is provided by  $K_0(t_i \hat{r}) \approx -\gamma - \ln(t_i \hat{r})$ , where  $\gamma = 0.5772$  is known as Euler's constant. In accordance with the fundamental solutions presented before, we have:

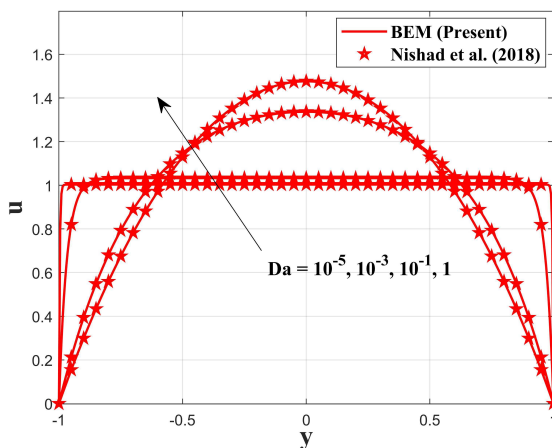
$$E_{jj} = \int_{q \in \Lambda_j^{(i)}} \frac{\partial G_i^{MH}(q_l, q)}{\partial n_q} ds - c_j = \frac{t_i}{2\pi} \int_{q \in \Lambda_j^{(i)}} K_1(t_i \hat{r}) \frac{\mathbf{r} \cdot \mathbf{n}}{\hat{r}} ds - c_j = -c_j, \quad (47)$$

Above said vectors namely,  $\mathbf{r}$  and  $\mathbf{n}$  are orthogonal to each other, which results in the vanishing of the integrals that appear above. In the same manner:

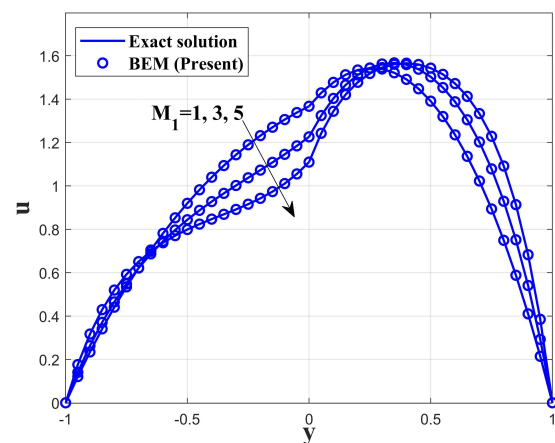
$$F_{jj} = - \int_{q \in \Lambda_j^{(i)}} G_i^C(q_l, q) ds = \frac{1}{2\pi} \int_{-0.5\tilde{l}_j}^{0.5\tilde{l}_j} \left[ \gamma + \ln \left( \frac{t_i \hat{r}}{2} \right) \right] d\hat{r} = \frac{\tilde{l}_j}{2\pi} \left[ \gamma + \ln \left( \frac{t_i \tilde{l}_j}{4} \right) - \frac{1}{t_i} \right], \quad (48)$$

$$C_{jj} = - \int_{q \in \Lambda_j^{(i)}} \frac{\partial G_i^C(q_l, q)}{\partial n_q} ds = -\frac{1}{t_i^2} \int_{q \in \Lambda_j^{(i)}} \left( \frac{\partial G_i^{MH}}{\partial n_q} - \frac{\partial G_i^L}{\partial n_q} \right) ds = 0, \quad (49)$$

$$D_{jj} = \int_{q \in \Lambda_j^{(i)}} G_i^C(q_l, q) ds = \frac{1}{t_i^2} \int_{q \in \Lambda_j^{(i)}} [G_i^{MH}(q_l, q) - G_i^L(q_l, q)] ds = \frac{1}{t_i^2} (F_{jj} - B_{jj}). \quad (50)$$



(a)  $\epsilon = 1$ ,  $M_1 = 10^{-4}$ ,  $\gamma = 1$ ,  $\alpha = 1$ ,  $\beta_1 = 0$ ,  $\beta_2 = 0$



(b)  $\epsilon = 1$ ,  $\gamma = 0.5$ ,  $\alpha = 0.4$ ,  $Da_1 = 1.5$ ,  $Da_2 = 1.7$ ,  $\beta_1 = \beta_2 = 0$

Fig. 3. Effect of (a) Darcy number, and (b) Hartman number on flow velocity.



**Table 1.**  $L^2$ - error corresponding to horizontal velocity for distinct values of Darcy number ( $Da$ )

Serial No.	Darcy Number ( $Da$ )	$L^2$ - error
1.	1	6.86E – 03
2.	$10^{-1}$	4.37E – 03
3.	$10^{-3}$	3.21E – 03
4.	$10^{-5}$	1.97E – 03

**Table 2.**  $L^2$ - error for horizontal velocity for distinct values of Hartman number ( $M_1$ )

Serial No.	Hartman number ( $M_1$ )	$L^2$ - error
1.	1	4.58E – 03
2.	3	2.39E – 03
3.	5	1.41E – 03

### 3. Results and Discussion

#### 3.1 Validation of BEM code

In absence of magnetic field (i.e.  $M_1 = 10^{-4}$ ) and taking the same porous material parameters in both the regions i.e., ( $Da_1 = Da_2$ ,  $\mu_1 = \mu_2$ ), the 2D flow of a viscous incompressible fluid through a composite porous channel is reduced to a single porous channel (please refer Fig. 3(a)). In this context, we have shown the impact of Darcy number on the flow velocity and compared the BEM results with the exact solution (Nishad et al. [31]) and observe that our result agrees very well with Nishad et al. [31]. This ensures the correctness of the BEM code. Next, we consider 2D fully developed flow of viscous incompressible fluid flow through a rectangular porous channel of distinct permeability. In this scenario, we have presented the influence of the Hartman number on flow velocity and compared our BEM solution with the corresponding exact solution. From Fig. 3(b), we determined that our BEM solution agrees with the exact solution (please refer to Appendix A). This further strengthens the correctness of BEM code.

#### 3.2 $L^2$ - error

To check the accuracy of the BEM code, we have determined the  $L^2$  - error corresponding to Fig. 3(a) and Fig. 3(b). The  $L^2$  - error in terms of velocity, for the steady value of  $\epsilon = 1$ ,  $M_1 = 10^{-4}$ ,  $\gamma = 1$ ,  $\alpha = 1$ ,  $\beta_1 = 0$ ,  $\beta_2 = 0$  and distinct values of Darcy number ( $Da$ ) i.e.,  $Da = 1$ ,  $10^{-1}$ ,  $10^{-3}$  and  $10^{-5}$  (please refer Table 1). The  $L^2$  - error for horizontal velocity is defined as:

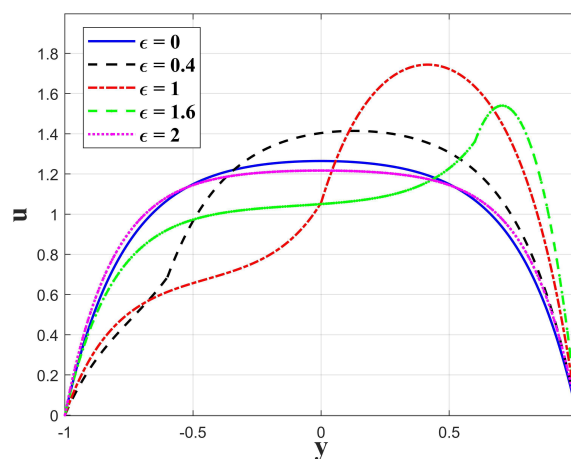
$$L^2 \text{ error} = \left[ \sum_{i=1}^{N_s} (u_E(i) - u_C(i))^2 \right]^{\frac{1}{2}} \quad (51)$$

where  $u_E$  and  $u_C$  denotes the exact and computed velocity and  $N_s$  denotes the number of solution points in the y-direction. By utilizing the above relation,  $L^2$  - error for horizontal velocity evaluated at the vertical centerline ( $x = 0$ ) corresponding to Fig. 3(a) is given in Table 1.

Similarly, for the steady value of  $\epsilon = 1$ ,  $\gamma = 0.5$ ,  $\alpha = 0.4$ ,  $Da_1 = 1.5$ ,  $Da_2 = 1.7$ ,  $\beta_1 = \beta_2 = 0$  and distinct values of Hartman number ( $M_1$ ) i.e.,  $M_1 = 1, 3$  and  $5$ , we have determined the  $L^2$  - error for horizontal velocity at the vertical centerline ( $x = 0$ ) corresponding to Fig. 3(b) is given in Table 2.

#### 3.3 Pressure-driven flow through 2D composite porous channel with applied transverse magnetic field

We assume 2D pressure-driven flow of a viscous, incompressible fluid through a channel consisting of two packings that are filled with fully saturated porous medium with an applied transverse magnetic field. It is assumed that the permeability of both porous packings has taken distinct. No-slip condition is applied on both walls of the channel. At the interface between two porous regions continuity of the velocity, a jump in shear stress and normal stress are applied. The dimension (length and breadth) of the rectangular channel is 10 and 2 units respectively (refer to Fig. 1).

**Fig. 4.** Influence of thickness parameter ( $\epsilon$ ) on velocity of fluid with  $\beta_1 = \beta_2 = 0$ .

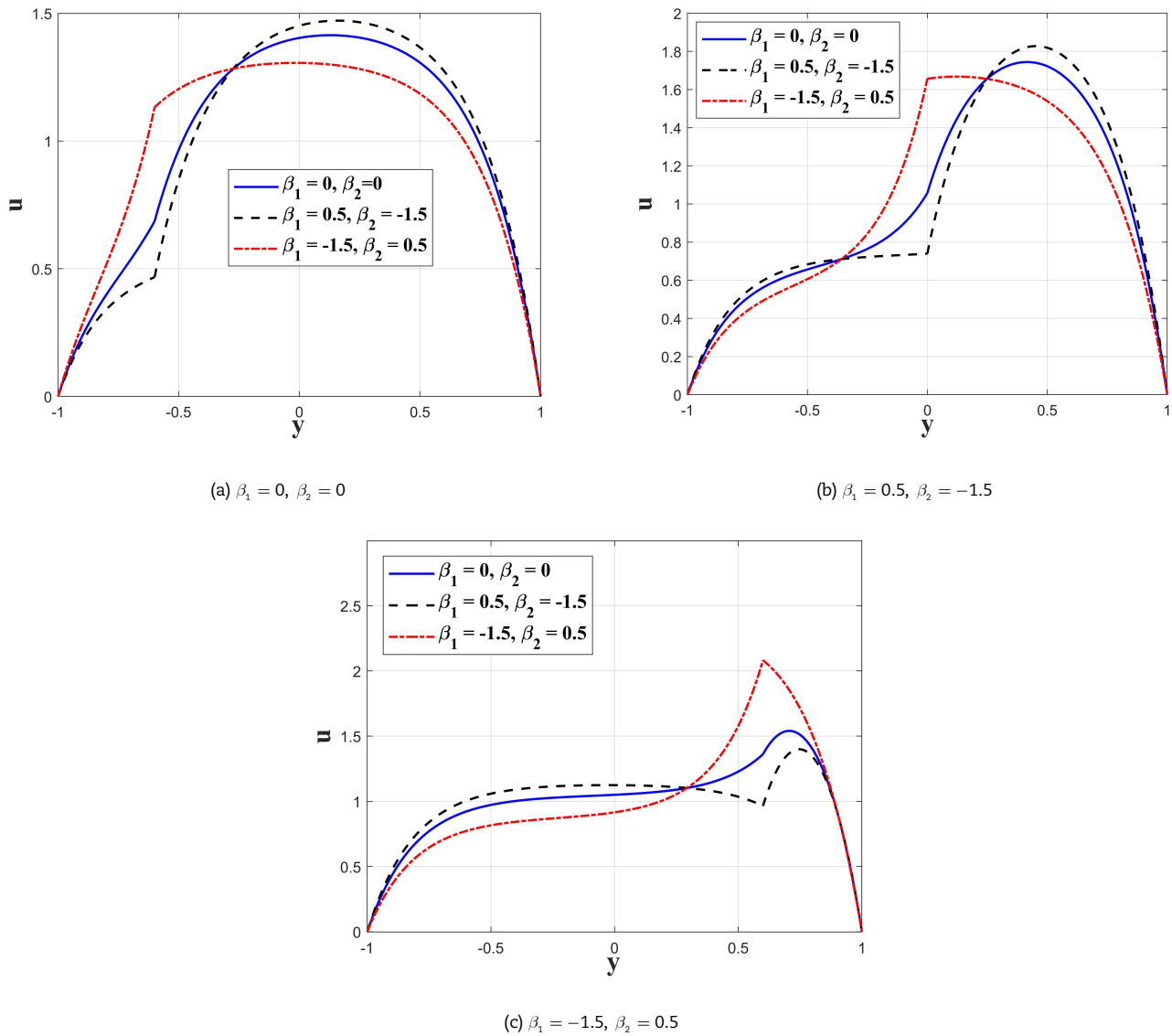


Fig. 5. Influence of Stress-jump coefficients on velocity of fluid with Hartman number  $M_1 = 3$ .

In Fig. 4, we have presented the impact of  $\epsilon$  ranging from 0 to 2 on flow velocity with  $Da_1 = 10^{-1}$ ,  $Da_2 = 5 \times 10^{-2}$ ,  $\alpha = 0.5$ ,  $\gamma = 0.5$ ,  $M_1 = 3$ . When  $\epsilon$  approaches either to 0 or 2, we observe that the channel consisting of two porous packings gets reduced to a single porous channel and the fluid velocity acquires its maxima at the middle portion and vanishes at the lower and upper surface due to no-slip condition. When  $\epsilon$  holds the value in between 0.4 and 1.6, the fluid velocity attains maxima in the upper region.

Next, in Fig. 5, we have presented the impact of stress-jump coefficients on the fluid velocity with distinct values of  $\epsilon$ ,  $M_1 = 3$ ,  $Da_1 = 10^{-1}$ ,  $Da_2 = 5 \times 10^{-2}$ ,  $\alpha = 0.5$ ,  $\gamma = 0.5$ . In every case we have taken three pairs of stress-jump coefficients  $(\beta_1, \beta_2)$  which are  $(0.5, -1.5)$ ,  $(0, 0)$  and  $(-1.5, 0.5)$ . We can notice from here that in considering pairs of  $(\beta_1, \beta_2)$ , when  $\beta_1$  increases from  $-1.5$  to  $0.5$ , at the same time  $\beta_2$  decrease from  $0.5$  to  $-1.5$ . From Fig. 5(a), we observed that when  $\epsilon = 0.4$ , as the  $\beta_1 \rightarrow -1.5$  to  $0.5$ , the flow velocity ( $u$ ) increases in the middle portion of the region  $\Omega^{(1)}$ , and then starts dropping from the interface ( $y = -0.6$ ) to the lower wall ( $y = -1$ ) of the porous packing  $\Omega^{(2)}$ . Next, in Fig. 5(b), we analyzed that when  $\epsilon = 1$ , and  $\beta_1 \rightarrow -1.5$  to  $0.5$ , horizontal velocity ( $u$ ) increases in  $\Omega^{(1)}$ , and decreases in  $\Omega^{(2)}$ . Lastly, in Fig. 5(c), When  $\epsilon = 1.6$  and  $\beta_1 < \beta_2$  (i.e., the case when  $\beta_1 = -1.5, \beta_2 = 0.5$ ), the velocity of the fluid becomes maximum closer to the interface ( $y = 0.4$ ), but when  $\beta_1 \neq \beta_2$  or  $\beta_1 > \beta_2$  (i.e., when  $\beta_1 = \beta_2 \neq 0$  or  $\beta_1 = 0.5, \beta_2 = -1.5$ ), flow velocity attains its maxima (maximum value of ( $u$ )) in comparison to all corresponding values of ( $u$ ) in the porous region  $\Omega^{(1)}$ , then decreases in the region  $\Omega^{(2)}$ . Also, we observed that there exist some points including point ( $y = -0.27$ ) in the region  $\Omega^{(2)}$  (please refer Fig. 5(a)), two points namely  $y = 0.25$  in the region  $\Omega^{(1)}$ , and  $y = -0.36$  in the region  $\Omega^{(2)}$  (please refer Fig. 5(b)), and point ( $y = 0.3$ ) in the region  $\Omega^{(2)}$  (refer to Fig. 5(c)), at which fluid velocity becomes independent of the variation of stress-jump coefficient, due to the existence of the boundary layer closer to the interface.

From Fig. 6(a) to Fig. 6(c), we analyzed that for the steady value of Hartman number ( $M_1 = 3$ ) while increasing the electrical conductivity  $\gamma$  from 0.25 to 1, fluid velocity increases in lower region  $\Omega^{(2)}$  and identically decreases in upper region  $\Omega^{(1)}$ , ( $y = 0$  to  $0.2$ ). The horizontal velocity ( $u$ ) remains uniform near the interface ( $y = 0$  to  $0.2$ ), this is because of the fact that increasing the electrical conductivity enhances the magnetic effect in upper porous region and suppresses the magnetic effect in lower region. There exists a point  $y = 0.2$ , where the horizontal velocity ( $u$ ) remains constant with increase in an electrical conductivity.





Next, in Fig. 7, we analyzed that for the steady value of Hartman number (i.e.  $M_1 = 3$ ), the horizontal velocity increases for the region ( $y = -1$  to  $0.1$ ) and decreases in the region ( $y = 0.1$  to  $1$ ) with increasing viscosity ratio  $\alpha$ , ranging from  $0.25$  to  $1$ . But when viscosity ratio  $\alpha$ , varies from  $1$  to  $1.75$ , the flow velocity starts dropping in the region  $\Omega^{(1)}$ , and increasing in the region  $\Omega^{(2)}$ . The horizontal velocity remains same near the interface ( $y = 0$ ).

Next, in Fig. 8 to Fig. 10, for the steady value of viscosity ratio ( $\alpha = 0.5$ ), Darcy number ( $Da_1 = 10^{-1}, Da_2 = 5 \times 10^{-2}$ ) and electrical conductivity ratio ( $\gamma = 0.5$ ), we have presented the influence of  $M_1$  on flow velocity with distinct values of  $\beta_1, \beta_2$  and  $\epsilon$ . We analyzed that increment in the value of  $M_1$  suppresses the velocity of the fluid along with three different cases of  $\beta_1, \beta_2$  with  $\epsilon = 0.4$  to  $1.6$ , which validates the prominent outcome that the magnetic field suppresses the fluid velocity. It takes place due to the applied magnetic field which acts perpendicular to the flow direction and is capable of generating force like Lorentz force which opposes the flow. When the Hartman number ( $M_1$ ) becomes very large i.e.,  $M_1 = 10, 15$ , and  $20$ , then horizontal velocity ( $u$ ) becomes uniform throughout the major part of the composite channel.

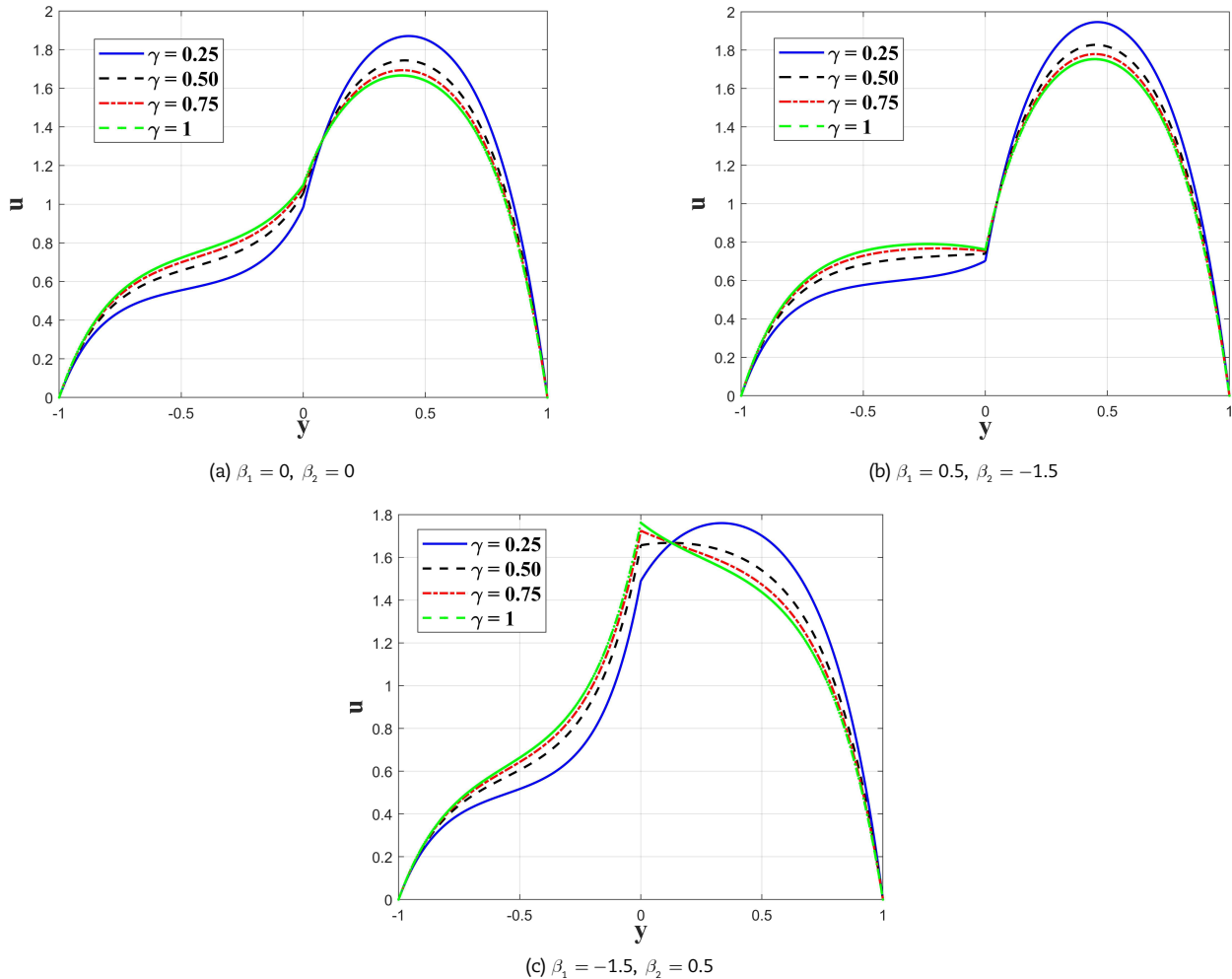


Fig. 6. Impact of electrical conductivity ratio on flow velocity with  $M_1 = 3$ ,  $\epsilon = 1$ ,  $\alpha = 0.5$ ,  $Da_1 = 10^{-1}$ ,  $Da_2 = 5 \times 10^{-2}$ .

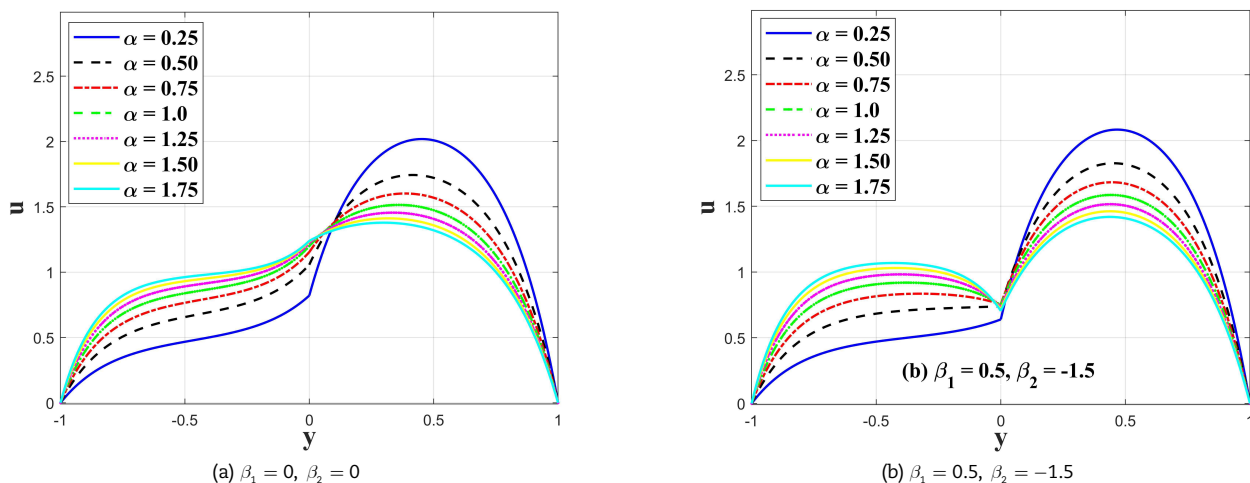


Fig. 7. Impact of viscosity ratio ( $\alpha$ ) on the velocity of fluid with  $M_1 = 3$ ,  $\epsilon = 1$ ,  $\gamma = 0.5$ ,  $Da_1 = 10^{-1}$ ,  $Da_2 = 5 \times 10^{-2}$ .



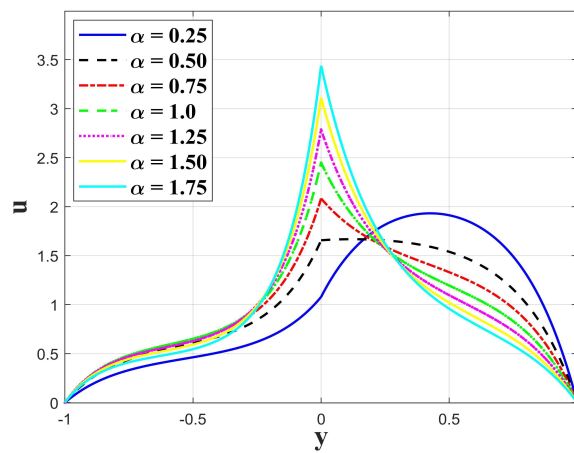
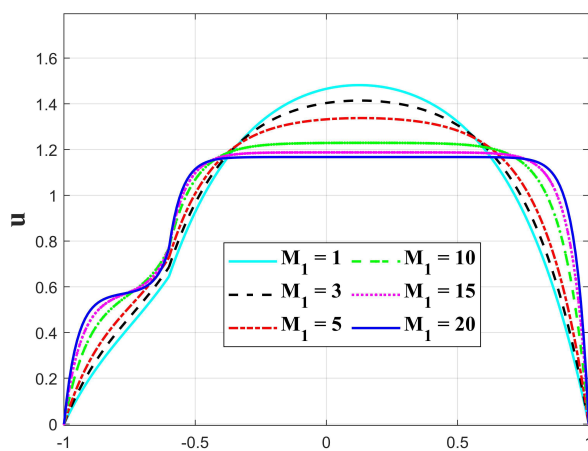
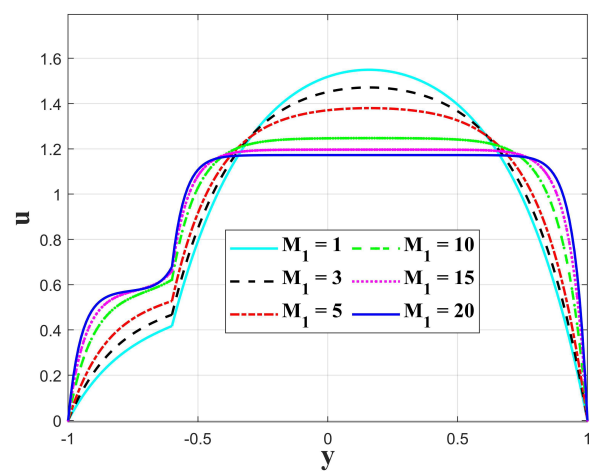
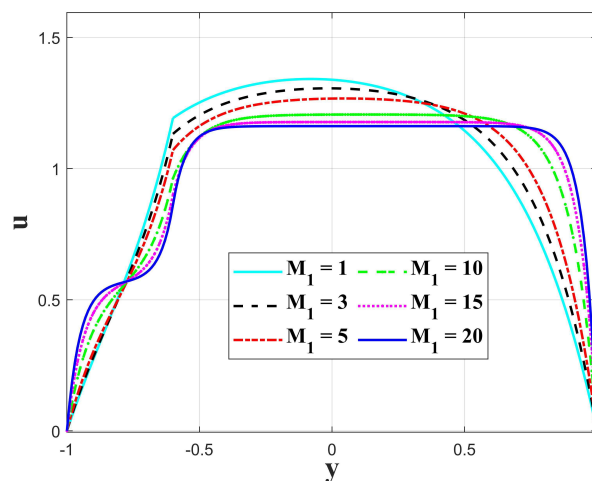
(c)  $\beta_1 = -1.5, \beta_2 = 0.5$ 

Fig. 7. Continued.

(a)  $\beta_1 = 0, \beta_2 = 0$ (b)  $\beta_1 = 0.5, \beta_2 = -1.5$ (c)  $\beta_1 = -1.5, \beta_2 = 0.5$ Fig. 8. Influence of Hartman number ( $M_1$ ) on velocity of the fluid with thickness parameter  $\epsilon = 0.4$ .

Next, from Fig. 8(a) to Fig. 8(c), we observe that as  $M_1$  rises, the fluid velocity drops in the middle portion ( $y = -0.6$  to  $0.6$ ) of the composite porous channel and increases near the lower ( $y = -1$  to  $-0.6$ ) and upper ( $y = 0.6$  to  $1$ ) surface to retain the constant volumetric flow. This is because of the fact that due to applied transverse magnetic field which acts in the normal flow direction, is high at the middle portion and low near the lower and upper surface. When the Hartman number increases, we observed that the slope of the tangent of the velocity field at the interface ( $y = 0$ ) is continuously changes due stress-jump condition.



From Fig. 9(a) to Fig. 9(c), we observe that as the Hartman number rises, the flow velocity amplifies near the boundary of the composite porous channel, in the portion ( $y = -1$  to  $-0.4$ ) and ( $y = 0.6$  to  $1$  approx.) in the region  $\Omega^{(2)}$  and  $\Omega^{(1)}$ , respectively. Also, the interesting aspect is that we noticed in Fig. 9(a), uniformity in the velocity of the fluid, in the portion ( $y = 0$  to  $0.1$ ) and at the point ( $y = -0.4$  approx.) is because of boundary layers formed in the vicinity of the upper and lower walls of the channel. In Fig. 9(a) and Fig. 9(c), by increasing the Hartman number ( $M_1$ ), flow velocity decreases in the portion ( $y = -0.4$  to  $0$ ) and ( $y = 0$  to  $0.6$ ) in porous regions  $\Omega^{(2)}$  and  $\Omega^{(1)}$ , respectively. From Fig. 9(b), we analyzed that on increasing the Hartman number ( $M_1$ ), horizontal velocity becomes ( $u$ ) uniform in the portion ( $y = -0.4$  to  $0.1$  approx.) and decreases in the portion ( $y = 0.1$  to  $0.7$ ) of the composite porous channel.

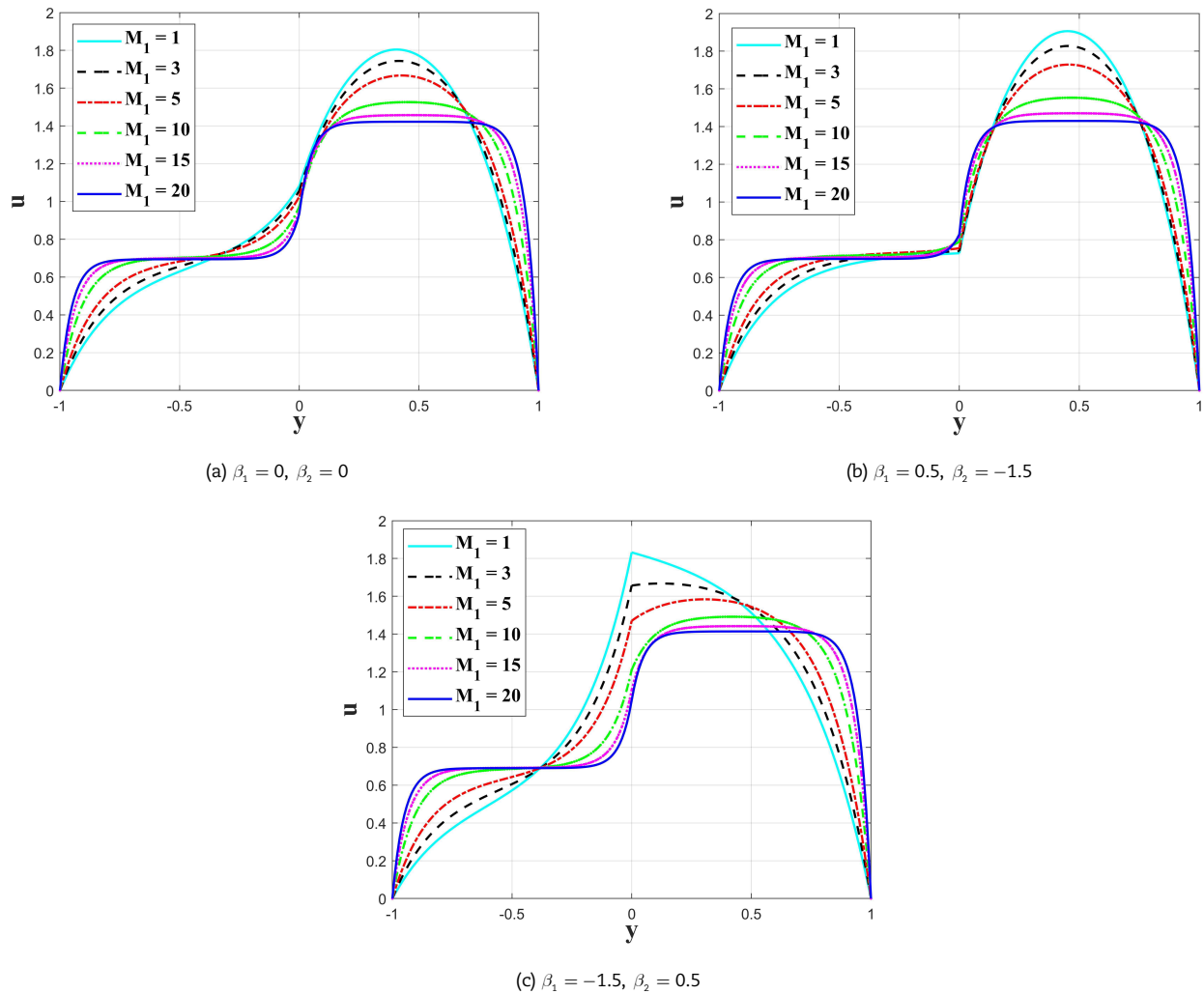


Fig. 9. Influence of Hartman number ( $M_1$ ) on velocity of the fluid with thickness parameter  $\epsilon = 1$ .

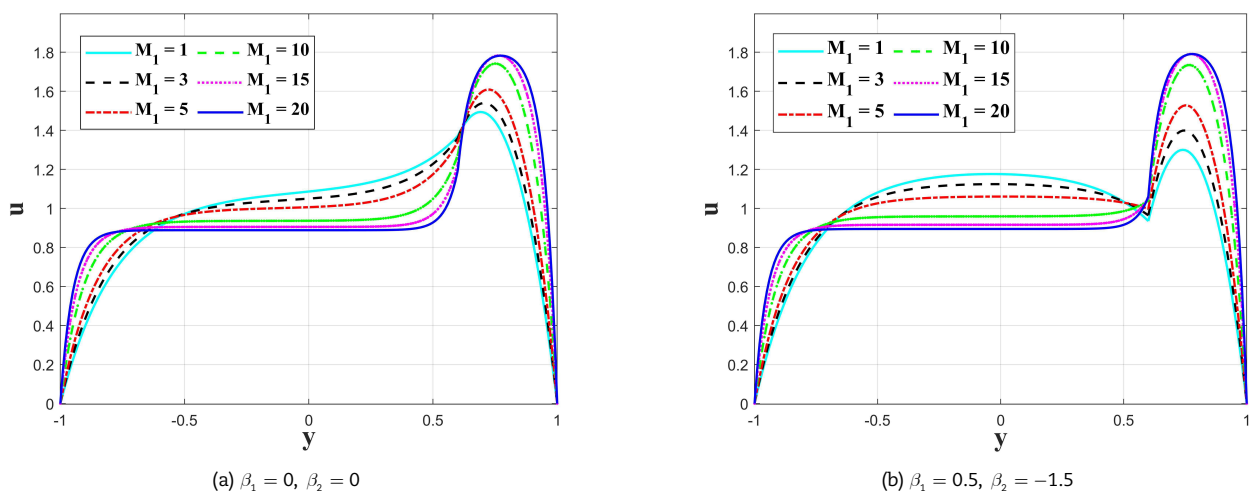
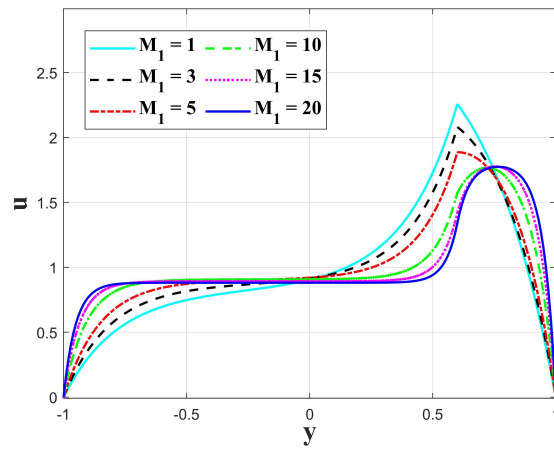


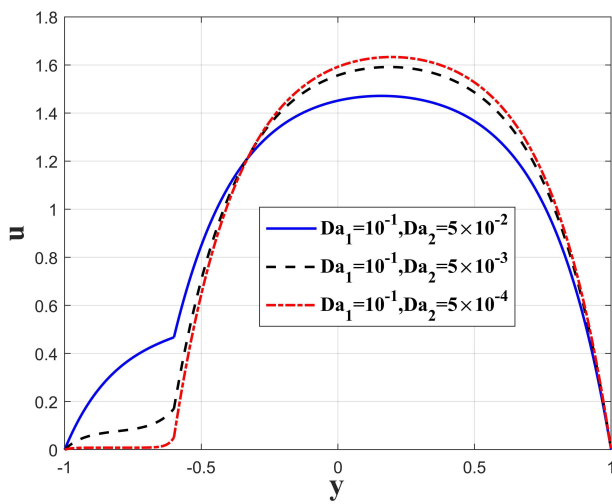
Fig. 10. Influence of Hartman number ( $M_1$ ) on velocity of the fluid with thickness parameter  $\epsilon = 1.6$ .



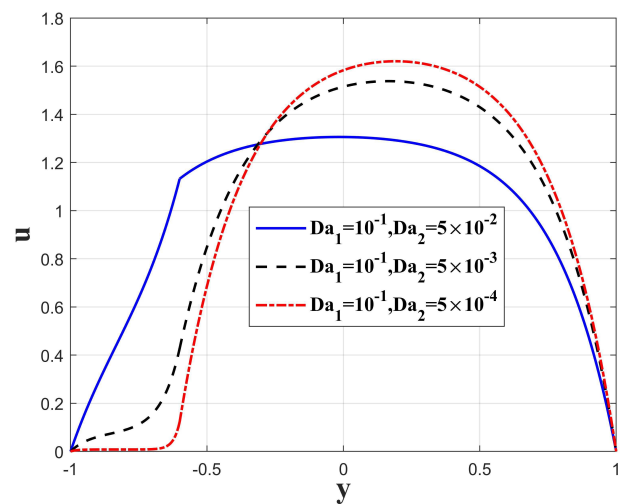


(c)  $\beta_1 = -1.5$ ,  $\beta_2 = 0.5$

Fig. 10. Continued.

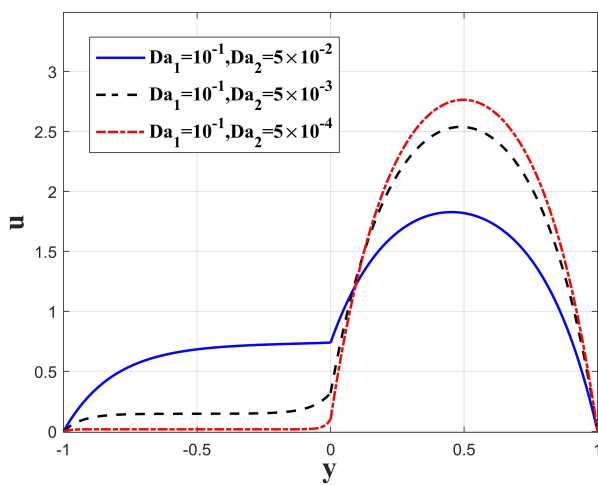


(a)  $\beta_1 = 0.5$ ,  $\beta_2 = -1.5$

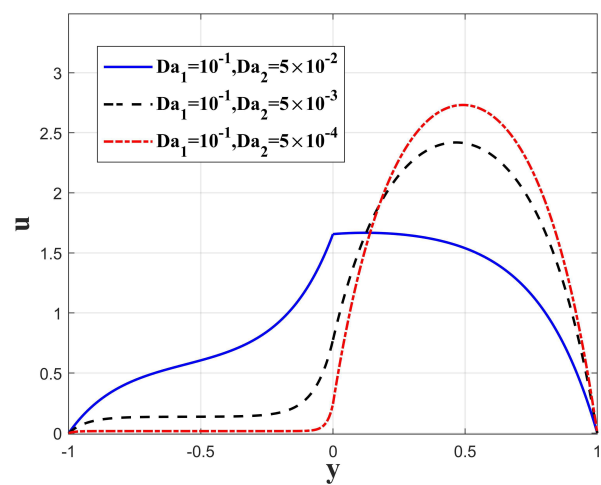


(b)  $\beta_1 = -1.5$ ,  $\beta_2 = 0.5$

Fig. 11. Impact of Darcy number on the fluid velocity with thickness parameter  $\epsilon = 0.4$ .



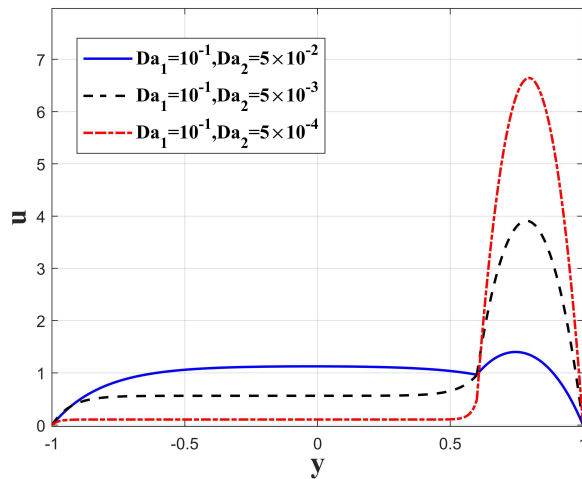
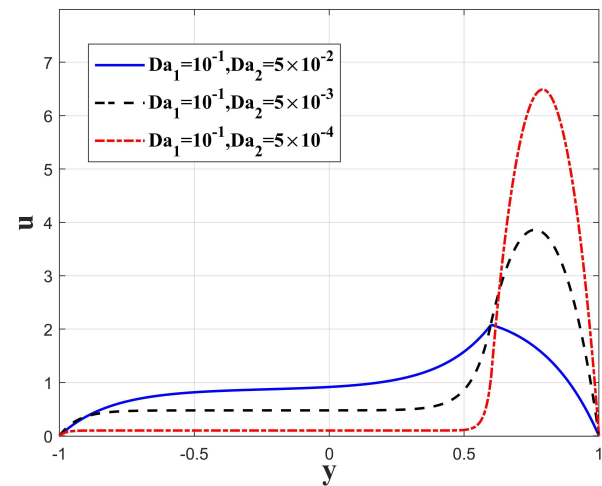
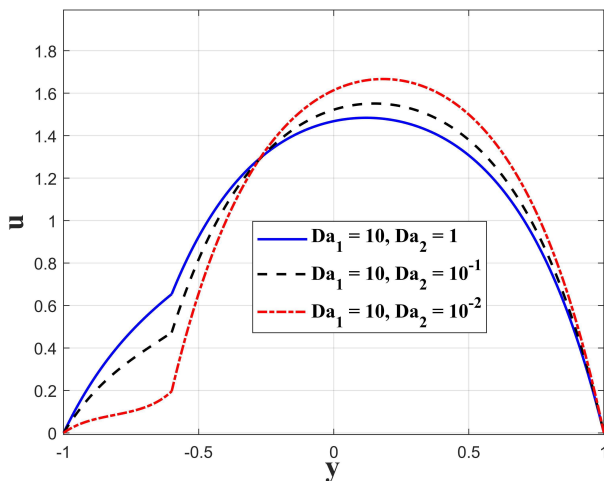
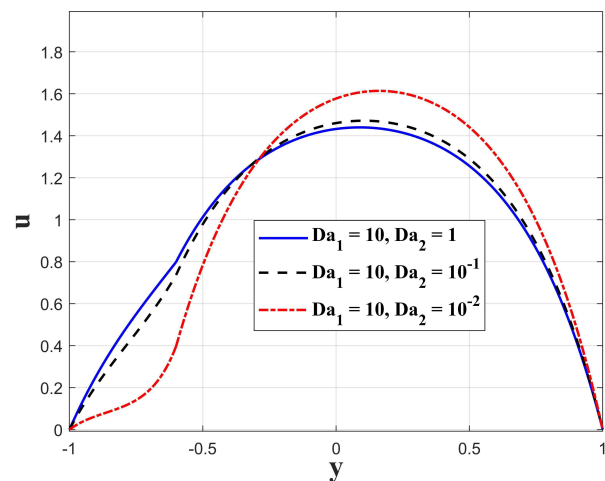
(a)  $\beta_1 = 0.5$ ,  $\beta_2 = -1.5$



(b)  $\beta_1 = -1.5$ ,  $\beta_2 = 0.5$

Fig. 12. Impact of Darcy number on fluid velocity with thickness parameter  $\epsilon = 1$ .



(a)  $\beta_1 = 0.5, \beta_2 = -1.5$ (b)  $\beta_1 = -1.5, \beta_2 = 0.5$ Fig. 13. Impact of Darcy number on fluid velocity with thickness parameter  $\epsilon = 1.6$ .(a)  $\beta_1 = 0.5, \beta_2 = -1.5$ (b)  $\beta_1 = -1.5, \beta_2 = 0.5$ Fig. 14. Impact of larger Darcy number fluid velocity with thickness parameter  $\epsilon = 0.4$ .

Next, In Fig. 10(a) and Fig. 10(b), we observe that by increasing the Hartman number ( $M_1$ ), flow velocity ( $u$ ) increases in the portion ( $y = -1$  to  $-0.6$  approx.) and ( $y = 0.6$  to  $1$ ) of porous region  $\Omega^{(2)}$  and  $\Omega^{(1)}$ , respectively. Parallely, flow velocity ( $u$ ) decreases in the middle portion ( $y = -0.6$  to  $0.6$  approx.) of the composite porous channel. In Fig. 10(c), we observe that by increasing the Hartman number ( $M_1$ ), flow velocity ( $u$ ) increases in the portion ( $y = -1$  to  $0$ ) and ( $y = 0.7$  to  $1$ ) of porous region  $\Omega^{(2)}$  and  $\Omega^{(1)}$ , respectively. Parallely, horizontal flow velocity ( $u$ ) decreases in the portion ( $y = 0$  to  $0.6$ ) and ( $y = 0.6$  to  $0.7$ ) of porous region  $\Omega^{(2)}$  and  $\Omega^{(1)}$ , respectively.

Next, in Fig. 11 to Fig. 14, for the steady value of Hartman number ( $M_1 = 3$ ), viscosity ratio ( $\alpha = 0.5$ ) and electrical conductivity ratio ( $\gamma = 0.5$ ), we have presented the influence of Darcy number ( $Da_1, Da_2$ ) on fluid velocity with distinct values of thickness parameter (here  $Da_1$  is fixed and  $Da_2$  varies), with described values of stress-jump coefficients. Here, we observed that for the steady value of Darcy number (e.g.  $Da_1 = 10^{-1}, Da_2 = 5 \times 10^{-2}$ ), when  $\beta_1 > \beta_2$ , the flow velocity increases in  $\Omega^{(1)}$  and decreases in  $\Omega^{(2)}$  in comparison to the case when  $\beta_1 < \beta_2$ , where flow velocity decreases in  $\Omega^{(1)}$  and increases in  $\Omega^{(2)}$  (please refer Fig. 11 to Fig. 13).

Similarly, we observed the same trend corresponding to a high Darcy number in Fig. 14, for both the cases when  $\beta_1 > \beta_2$ , and  $\beta_1 < \beta_2$ , where  $\epsilon = 0.4$ . This happens because the porous packing below the interface in the channel provides resistance by virtue of its reduced permeability relative to the porous packing upper to the interface of the channel. Also, we observe that there exists a point  $y = 0.6$  (please refer Fig. 13),  $y = 0.1$  approx. (please refer Fig. 12) and  $y = -0.3$  approx. (please refer Fig. 11 and Fig. 14), on which the velocity ( $u$ ) remains constant. This occurs because of the existence of the boundary layer closer to the interface.

Next, Fig. 15(a) presents influence of  $\beta_1$  and  $\beta_2$  on the interfacial velocity of the fluid against the thickness parameter with distinct values of  $\beta_1, \beta_2$  and  $M_1 = 3, Da_1 = 10^{-1}, Da_2 = 5 \times 10^{-2}, \alpha = 0.5, \gamma = 0.5$ . We observe that when  $\epsilon \rightarrow 0$  or  $2$ , the interfacial velocity vanishes at the top and bottom non-permeable surface of the channel because of the applied no-slip condition. We analyzed that  $\beta_1$  and  $\beta_2$  strongly affects the flow velocity ( $u$ ) at the interface i.e., interfacial velocity increases with an increment in stress-jump coefficient. In Fig. 15(b), we observed the existence of two boundary layers, one below the interface and one above the interface of both porous regions of thickness  $\delta_1$  and  $\delta_2$ , respectively. So, in this manner, we can determine the modified Brinkman layer of thickness  $\delta_{mod} = \delta_1 + \delta_2$  closer to the interface of the channel.





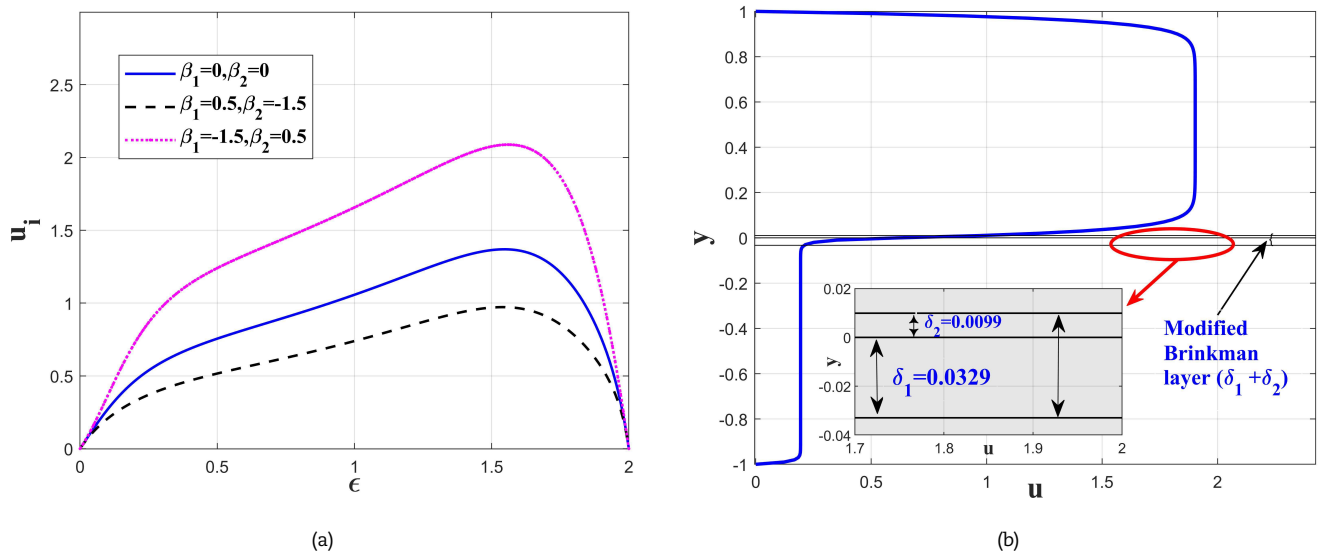


Fig. 15. (a) Influence of stress-jump coefficients ( $\beta_1, \beta_2$ ) on the interfacial velocity of the fluid against thickness parameter, (b) Appearance of Brinkman layer of thickness ( $\delta_1 + \delta_2$ ) corresponding to  $M_1 = 5$ ,  $Da_1 = 10^{-3}$ ,  $Da_2 = 10^{-4}$ ,  $\epsilon = 1$ ,  $\mu_1 = 1$ ,  $\mu_2 = 1$ ,  $\beta_1 = 1.5$ ,  $\beta_2 = 0.5$ ,  $\gamma = 0.5$ .

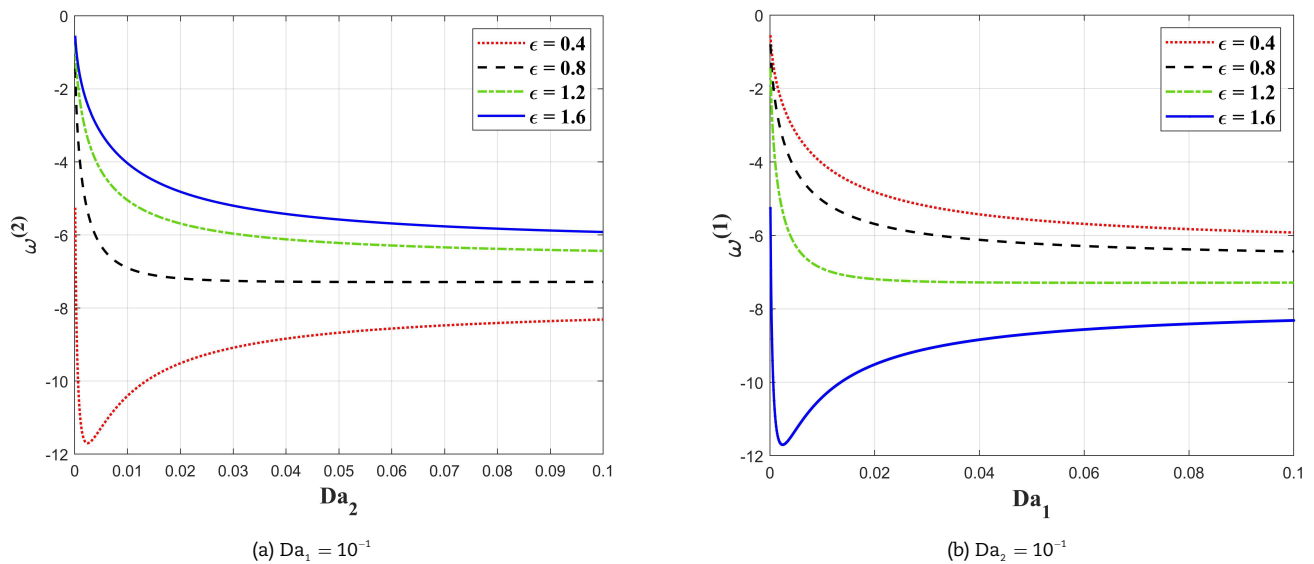


Fig. 16. Influence of thickness parameter ( $\epsilon$ ) on flow vorticity  $\omega^{(i)}$ . (a) flow vorticity at the bottom wall for  $Da_1 = 10^{-1}$ , (b) flow vorticity at the top wall for  $Da_2 = 10^{-1}$ .

Next, in Fig. (16), for the steady values of stress-jump coefficient ( $\beta_1 = \beta_2 = 0$ ), Hartman number ( $M_1 = 5$ ), electrical conductivity ( $\gamma = 0.5$ ), and viscosity ( $\alpha = 1$ ), we have shown the impact of Darcy number ( $Da$ ) on flow vorticity ( $\omega$ ) for distinct values of thickness parameter ( $\epsilon$ ). Figure 16(a) shows that flow vorticity at the lower surface varies with  $Da_2$  for distinct values of  $\epsilon$ . For a steady value of  $\epsilon$ , we observe that the magnitude of vorticity at the lower and upper walls increases with increasing Darcy number. This is because a high Darcy number results in high velocity near the walls, which in turn leads to high vorticity at the walls. The drop of flow vorticity at the lower wall, owing to the decrease in available volume flux within the lower porous region as the thickness parameter ( $\epsilon$ ) increases. The equilibrium of volume flux ensures the amplification of flow vorticity at the upper wall, as demonstrated in Fig. 16(b).

### 3.4 Investigation of Brinkman layer thickness

We have computed Brinkman layer thickness  $\delta_1$  and  $\delta_2$  near the interface (please refer Appendix B), for both the regions  $\Omega^{(i)}$  for  $i = 1, 2$  as a function of transport parameters presented in Table 3. We observed that  $\delta_1$  and  $\delta_2$  strongly depends on the flow parameters. For example, when  $M_1 = 5$ , for the steady values of  $(\mu_1, \mu_2)$  and  $(\beta_1, \beta_2)$ , distinct porous materials including Foametal, Aloxite etc. [12], have been discussed and it is obtained that by rising the value of Darcy number ( $Da_1, Da_2$ ), there is an increase in Brinkman layer thickness. In this context, if we take  $M_1 = 12$  and 20, it is observed that Brinkman layer thickness is greater in the case when  $M_1 = 20$  than the case when  $M_1 = 5$  or 12, with increasing Darcy number. Finally, we conclude from here that Brinkman layer thickness increases with the Hartman number as well as the Darcy number for the steady values of  $(\mu_1, \mu_2)$  and  $(\beta_1, \beta_2)$ .



**Table 3.** Thickness of Brinkman layer for distinct porous material.

Hartman number ( $M_1$ )	Darcy number ( $Da_1, Da_2$ )	Viscosity ( $\mu_1, \mu_2$ )	Stress-jump coefficient ( $\beta_1, \beta_2$ )	Brinkman-layer thickness ( $\delta_1, \delta_2$ )
$M_1 = 5$	(Foametal (1), Aloxite (2)) ( $8.2 \times 10^{-4}$ , $1.6 \times 10^{-5}$ )	(10, 4)	(1.5, 0.5)	(0.0308, 0.0042)
	(Foametal (1), Aloxite (2)) ( $1.6 \times 10^{-5}$ , $8.2 \times 10^{-4}$ )	(4, 10)	(0.5, 1.5)	(0.0040, 0.0873)
	( $10^{-3}$ , $10^{-4}$ )	(10, 4)	(1.5, 0.5)	(0.0340, 0.0142)
	( $10^{-4}$ , $10^{-3}$ )	(4, 10)	(0.5, 1.5)	(0.0099, 0.1479)
	( $10^{-2}$ , $10^{-3}$ )	(10, 4)	(1.5, 0.5)	(0.1524, 0.0428)
$M_1 = 12$	(Foametal (1), Aloxite (2)) ( $8.2 \times 10^{-4}$ , $1.6 \times 10^{-5}$ )	(10, 4)	(1.5, 0.5)	(0.0372, 0.0042)
	(Foametal (1), Aloxite (2)) ( $1.6 \times 10^{-5}$ , $8.2 \times 10^{-4}$ )	(4, 10)	(0.5, 1.5)	(0.0040, 0.0920)
	( $10^{-3}$ , $10^{-4}$ )	(10, 4)	(1.5, 0.5)	(0.0416, 0.0138)
	( $10^{-4}$ , $10^{-3}$ )	(4, 10)	(0.5, 1.5)	(0.0097, 0.1643)
	( $10^{-2}$ , $10^{-3}$ )	(10, 4)	(1.5, 0.5)	(0.3615, 0.0320)
$M_1 = 20$	(Foametal (1), Aloxite (2)) ( $8.2 \times 10^{-4}$ , $1.6 \times 10^{-5}$ )	(10, 4)	(1.5, 0.5)	(0.0508, 0.0042)
	(Foametal (1), Aloxite (2)) ( $1.6 \times 10^{-5}$ , $8.2 \times 10^{-4}$ )	(4, 10)	(0.5, 1.5)	(0.0040, 0.1018)
	( $10^{-3}$ , $10^{-4}$ )	(10, 4)	(1.5, 0.5)	(0.0573, 0.0131)
	( $10^{-4}$ , $10^{-3}$ )	(4, 10)	(0.5, 1.5)	(0.0093, 0.2013)
	( $10^{-2}$ , $10^{-3}$ )	(10, 4)	(1.5, 0.5)	(0.7024, 0.0130)

#### 4. Conclusion

We have analyzed the impact of magnetic field on steady 2D viscous, incompressible flow through composite porous channel consisting of two porous packings having distinct permeabilities using the non-primitive boundary element method. The employment of non-primitive variables-based BEM exhibits several merits over the primitive variables-based BEM approach, including but not limited to: (a) the stream function satisfies the continuity equation intrinsically, and (b) the pressure term is eliminated from the momentum equation. Despite the notable advantages, the employment of non-primitive variables based BEM approach in certain physical systems has inherent drawbacks, namely, (a) the 3D extension is not always amenable to straightforward treatment and often necessitates additional variables, (b) the explicit computation of the pressure field is not always feasible, and (c) non-primitive variables are not optimally suited to address problems that feature corner singularities, thereby warranting specialized treatment. It is found that thickness parameter, stress-jump coefficient, electrical conductivity ratio, fluid viscosity ratio, and Hartman number have strong impact on fluid mechanics. We observed that the thickness parameter has an impact on the fluid flow. This understanding is essential for the design and analysis of porous media-based systems, as well as for optimizing the performance of various industrial applications including mass transfer and mixing enhancement. Also, we observed that horizontal velocity decreases as the Hartman number increases. This phenomenon occurs as a consequence of an applied magnetic field that is orthogonal to the direction of flow. It is also observed that as the electrical conductivity ratio amplifies, the velocity distribution remains steadfastly uniform in the vicinity of the interface, owing to the augmentation of electrical conductivity, which in turn reinforces the magnetic field in the corresponding regions. An escalation in the stress-jump coefficient produces a corresponding amplification in the interfacial velocity. We observed that for a steady value of thickness parameter, the magnitude of vorticity (at the lower and upper walls) increases with increasing Darcy number. Also, we observed that the magnitude of vorticity at lower wall decreases and at upper wall increases with increasing thickness parameter. We have computed Brinkman layer thickness near the interface and observed that Brinkman layer thickness is strongly dependent on the Hartman number, Darcy number, viscosity, and stress-jump coefficient, respectively.

#### Author Contributions

V. Chhabra: Developing the MATLAB code, Validation, Investigation, Writing the manuscript, C.S. Nishad: Methodology, Investigation, Supervision, Writing the manuscript, M. Sahni: Methodology, Investigation, and Supervision. All authors discussed the results, reviewed, and approved the final version of the manuscript.



## Acknowledgments

The author Vishal is thankful for the financial support from Pandit Deendayal Energy University, Gujarat, India, in a form of fellowship offered by the institute.

## Conflict of Interest

The authors have no conflict of interest.

## Funding

The authors received no financial support for the research, authorship, and publication of this article.

## Data Availability Statements

The datasets generated and/or analyzed during the current study are available from the corresponding author on reasonable request.

## Nomenclature

$\vec{B}$	Magnetic induction vector of the applied uniform	$\alpha$	Fluid viscosity ratio
$Da_1, Da_2$	Darcy number of the porous medium	$\beta_1, \beta_2$	Stress-jump coefficients
$\vec{F}$	Lorentz force	$\gamma$	Electrical conductivity ratio
$G^C$	Free space Green's function for mixed Laplace and modified Helmholtz equation	$\delta_1, \delta_2$	Brinkman layer thickness
$G^L$	Free space Green's function for Laplace equation	$\epsilon$	Thickness parameter
$G^{MH}$	Free space Green's function for modified Helmholtz equation	$\Lambda^{(1)}, \Lambda^{(2)}$	Boundary of the porous regions
$\vec{H}$	Characteristic length	$\tilde{\mu}$	Fluid viscosity
$\vec{j}$	Density of electric current	$\tilde{\mu}_e$	Effective viscosity of the porous matrix
$\vec{k}_1, \vec{k}_2$	Permeability of the porous regions	$\vec{\sigma}$	Electrical conductivity of the fluid
$K_0$	Modified Bessel function	$\psi$	Stream function
$M_1, M_2$	Hartman number	$\Omega^{(1)}, \Omega^{(2)}$	Porous regions
$\tilde{p}$	Hydrodynamics pressure	$\omega$	Vorticity variable
$\vec{U}$	Characteristic velocity	$d\vec{p} / d\vec{x}$	Pressure gradient
$\vec{v}$	Fluid velocity		

## References

- [1] Kuznetsov, A.V., Analytical Investigation of the Fluid Flow in the Interface Region between a Porous Medium and a Clear Fluid in Channels Partially Filled with a Porous Medium, *Flow, Turbulence and Combustion*, 56, 1996, 53–67.
- [2] Yu, P., Lee, T.S., Zeng, Y., Low, H.T., A Numerical Method for Flows in Porous and Homogenous Fluid Domains Coupled at the Interface by Stress Jump, *International Journal for Numerical Methods in Fluids*, 53(11), 2007, 1755–1775.
- [3] Tan, H., Pillai, K.M., Finite Element Implementation of Stress-Jump and Stress-Continuity Conditions at Porous-Medium, clear-fluid interface, *Computers & Fluids*, 38(6), 2009, 1118–1131.
- [4] Yadav, P.K., Jaiswal, S., Influence of an Inclined Magnetic Field on the Poiseuille Flow of Immiscible Micropolar-Newtonian Fluids in a Porous Medium, *Canadian Journal of Physics*, 96(9), 2018, 1016–1028.
- [5] Yadav, P.K., Jaiswal, S., Verma, A.K., Chamkha, A.J., Magnetohydrodynamics of Immiscible Newtonian Fluids in Porous Regions of Different Variable Permeability Functions, *Journal of Petroleum Science and Engineering*, 220(B), 2023, 111113.
- [6] Allan, F.M., Hamdan, M.H., Fluid Mechanics of the Interface Region between Two Porous Layers, *Applied Mathematics and Computation*, 128(1), 2002, 37–43.
- [7] Turkyilmazoglu, M., Exact Solutions for the Incompressible Viscous Fluid of a Porous Rotating Disk Flow, *International Journal of Non-Linear Mechanics*, 44(4), 2009, 352–357.
- [8] Turkyilmazoglu, M., A direct Solution of Temperature Field and Physical Quantities for the Nonlinear Porous Fin Problem, *International Journal of Numerical Methods for Heat & Fluid Flow*, 27(2), 2017, 516–529.
- [9] Yadav, P.K., Verma, A.K., Analysis of Two Immiscible Newtonian and Micropolar Fluid Flow through an Inclined Porous Channel, *Mathematical Methods in the Applied Science*, 45(3), 2022, 1700–1724.
- [10] Ochoa-Tapia, J.A., Whitaker, S., Momentum Transfer at the Boundary between a Porous Medium and a Homogeneous Fluid—I. Theoretical development, *International Journal of Heat and Mass Transfer*, 38(14), 1995, 2635–2646.
- [11] Ochoa-Tapia, J.A., Whitaker, S., Momentum Transfer at the Boundary between a Porous Medium and a Homogeneous Fluid—II. Comparison with experiment, *International Journal of Heat and Mass Transfer*, 38(14), 1995, 2647–2655.
- [12] Neale, G.H., Nader, W.K., Practical Significance of Brinkman Extension of Darcy's Law, *The Canadian Journal of Chemical Engineering*, 52, 1974, 475–478.
- [13] Ahmadi, E., Cortez, R., Fujioka, H., Boundary Integral Formulation for Flows Containing an Interface between Two Porous Media, *Journal of Fluid Mechanics*, 816, 2017, 71–93.
- [14] Turkyilmazoglu, M., Velocity Slip and Entropy Generation Phenomena in Thermal Transport through Metallic Porous Channel, *Journal of Non-Equilibrium Thermodynamics*, 45(3), 2020, 247–256.
- [15] Ge-Jile, H., Nazeer, M., Hussain, F., Khan, M.I., Saleem, A., Siddique, I., Two-phase Flow of MHD Jeffrey Fluid with the Suspension of Tiny Metallic Particles Incorporated with Viscous Dissipation and Porous Medium, *Advances in Mechanical Engineering*, 13(3), 2021, 1–15.
- [16] Han Aydin, S., Selvitopi, H., Stabilized FEM–BEM Coupled Solution of MHD Pipe Flow in an Unbounded Conducting Medium, *Engineering Analysis with Boundary Elements*, 87, 2017, 122–132.
- [17] Bali, R., Awasthi, U., Effect of a Magnetic Field on the Resistance to Blood Flow through Stenotic Artery, *Applied Mathematics and Computation*, 188(2), 2007, 1635–1641.
- [18] Verma, V.K., Datta, S., Magnetohydrodynamic Flow in a Channel with Varying Viscosity under Transverse Magnetic Field, *Advances in Theoretical and Applied Mechanics*, 3(2), 2010, 53–66.
- [19] Tiwari, A., Deo, S., Filippov, A., Effect of the Magnetic Field on the Hydrodynamic Permeability of a Membrane, *Colloid Journal*, 74(4), 2012, 515–522.
- [20] Manyonge, W.A., Kiema, D.W., Iyaya, C.C.W., Steady MHD Poiseuille Flow between Two Infinite Parallel Porous Plates in an Inclined Magnetic Field, *International Journal of Pure and Applied Mathematics*, 76(5), 2012, 661–668.
- [21] Ansari, I.A., Deo, S., Effect of Magnetic Field on the Two Immiscible Viscous Fluids Flow in a Channel Filled with Porous Medium, *National Journal of Applied and Computational Mechanics*, Vol. 9, No. 4, (2023), 1016–1035



Academy Science Letters, 40(3), 2017, 211–214.

[22] Wahid, N.S., Arifin, N.M., Turkyilmazoglu, M., Rahmin, N.A.A., Hafidzuddin, M.E.H., Effect of Magnetohydrodynamic Casson Fluid Flow and Heat Transfer Past a Stretching Surface in Porous Medium with Slip Condition, *IOP Publishing*, 2019.

[23] Yadav, P.K., Jaiswal, S., Puchakatla, J.Y., Micropolar Fluid Flow through the Membrane Composed of Impermeable Cylindrical Particles Coated by Porous Layer Under the Effect of Magnetic Field, *Mathematical Methods in the Applied Sciences*, 43(4), 2020, 1925–1937.

[24] Jaiswal, S., Yadav, P.K., A Micropolar-Newtonian Blood Flow Model through a Porous Layered Artery in the Presence of a Magnetic Field, *Physics of Fluids*, 31(7), 2019, 071901.

[25] Yadav, P.K., Verma, A.K., Analysis of Two Non-Miscible Electrically Conducting Micropolar Fluid Flow through an Inclined Porous Channel: Influence of Magnetic Field, *ZAMM – Journal of Applied Mathematics and Mechanics*, 103, 2022, e202200047.

[26] Selvitopi, H., Stabilized FEM Solution of Magnetohydrodynamics Flow in Different Geometries, *Journal of Scientific Reports-A*, 49, 2022, 105–117.

[27] Selvitopi, H., Numerical Investigation of Damped Wave type MHD Flow with Time-Varied External Magnetic Field, *Chinese Journal of Physics*, 80, 2022, 127–147.

[28] Nishad, C.S., Karmakar, T., Chandra, A., Raja Sekhar, G.P., A Non-Primitive Boundary Integral Formulation for Modeling Flow through Composite Porous Channel, *Engineering Analysis with Boundary Elements*, 109, 2019, 94–105.

[29] Srivastava, B.G., Deo, S., Effect of Magnetic Field on the Viscous Fluid Flow in a Channel Filled with Porous Medium of Variable Permeability, *Applied Mathematics and Computation*, 219(17), 2013, 8959–8964.

[30] Tezduyar, T.E., Liou, J., Ganjoo, D.K., Incompressible Flow Computations based on the vorticity-stream Function and Velocity-pressure Formulations, *Computers & Structures*, 35(4), 1990, 445–472.

[31] Nishad, C.S., Karmakar, T., Chandra, A., Raja Sekhar, G.P., A Non-Primitive Boundary Element Technique for Modeling Flow through Non-Deformable Porous Medium using Brinkman Equation, *Meccanica*, 53(9), 2018, 2333–2352.

[32] Grosan, T., Postelnicu, A., Pop, I., Brinkman Flow of a Viscous Fluid through a Spherical Porous Medium Embedded in Another Porous Medium, *Transport in Porous Media*, 81(1), 2010, 89–103.

[33] Katsikadelis, J.T., *Boundary Elements: Theory and Applications*, Elsevier, Amsterdam, 2002.

[34] Nishad, C.S., Chandra, A., Raja Shekhar, G.P., Stokes Flow Inside Topographically Patterned Microchannel Using Boundary Element Method, *International Journal of Chemical Reactor Engineering*, 15(5), 2017, 1–17.

[35] Goharzadeh, A., Saidi, A., Wang, D., Merzkirch, W., Khalili, A., An Experimental Investigation of the Brinkman Layer Thickness at a Fluid-Porous Interface, *Solid Mechanics and its Applications*, 129, 2006, 445–454.

## Appendix A. Evaluation of velocity of the fluid for 2D flow through composite porous channel

The governing equations of corresponding 2D fully developed flow in above and below the interface of the channel are as follows:

$$\frac{d^2 u_1}{dy^2} - t_1^2 u_1 = P, \quad -1 + \epsilon \leq y \leq 1, \quad (A1)$$

$$\frac{d^2 u_2}{dy^2} - t_2^2 u_2 = \alpha P, \quad -1 \leq y \leq -1 + \epsilon. \quad (A2)$$

General solution corresponding to Eqs. (A1)-(A2) is given by:

$$u_1(y) = A \cosh(t_1 y) + B \sinh(t_1 y) - \frac{P}{t_1^2}, \quad -1 + \epsilon \leq y \leq 1, \quad (A3)$$

$$u_2(y) = C \cosh(t_2 y) + D \sinh(t_2 y) - \frac{\alpha P}{t_2^2}, \quad -1 \leq y \leq -1 + \epsilon. \quad (A4)$$

where  $P = dp/dx$ ,  $t_i^2 = (\eta_i^2 + M^2)$ , ( $i = 1, 2$ ). Here, we assume  $\eta = -1 + \epsilon$ .

For finding the exact values of A, B, C, and D appearing in Eqs. (A3)-(A4), we applied no-slip boundary condition at the upper ( $y = 1$ ) and the lower ( $y = -1$ ) surfaces of the channel, continuity of velocity, and jump in shear stress at the interface ( $y = \eta$ ), given by:

$$u_1|_{y=1} = 0, \quad u_2|_{y=-1} = 0 \quad (A5)$$

$$u_1|_{y=\eta} = u_2|_{y=\eta} \quad (A6)$$

$$\mu_1 \frac{du_1}{dy} - \mu_2 \frac{du_2}{dy} = \alpha_1 u_1 \quad (A7)$$

$$\text{where } \alpha_1 = \mu_1 \left[ \frac{\beta_1}{\sqrt{Da_1}} - \frac{\beta_2}{\sqrt{Da_2}} \right].$$

The closed form of the flow velocity in  $\Omega^{(1)}$  and  $\Omega^{(2)}$  is given by:

$$u_1(y) = MP [\sinh(t_1 y) - \tanh(t_1) \cosh(t_1 y)] + \frac{P \cosh(t_1 y)}{t_1^2 \cosh(t_1)} - \frac{P}{t_1^2}, \quad (A8)$$

$$u_2(y) = NP [\sinh(t_2 y) + \tanh(t_2) \cosh(t_2 y)] + \frac{\alpha P \cosh(t_2 y)}{t_2^2 \cosh(t_2)} - \frac{\alpha P}{t_2^2}. \quad (A9)$$



Denoting:

$$E(s) = \cosh\{t_1(s)\} - \tanh(t_1)\sinh\{t_1(s)\}, \quad (A10)$$

$$F(s) = \sinh\{t_1(s)\} - \tanh(t_1)\cosh\{t_1(s)\}, \quad (A11)$$

$$G(s) = \cosh\{t_2(s)\} + \tanh(t_2)\sinh\{t_2(s)\}, \quad (A12)$$

$$H(s) = \sinh\{t_2(s)\} + \tanh(t_2)\cosh\{t_2(s)\}, \quad (A13)$$

$$I(s) = F(s) - \frac{\alpha t_1 E(s) H(s)}{t_2 G(s)} + \frac{\alpha_1 F(s) H(s)}{\mu_2 t_2 G(s)}, \quad (A14)$$

$$M = \frac{\alpha \cosh(t_2 \eta)}{t_2^2 I(\eta) \cosh(t_2)} - \frac{\alpha}{t_2^2 I(\eta)} - \frac{\cosh(t_1 \eta)}{t_1^2 I(\eta) \cosh(t_1)} + \frac{1}{t_1^2 I(\eta)} + \frac{\alpha H(\eta) \sinh(t_1 \eta)}{t_1 t_2 G(\eta) I(\eta) \cosh(t_1)} - \frac{\alpha H(\eta) \sinh(t_2 \eta)}{t_2^2 G(\eta) I(\eta) \cosh(t_2)} - \frac{\alpha_1 H(\eta) \cosh(t_1 \eta)}{\mu_2 t_1^2 t_2 G(\eta) I(\eta) \cosh(t_1)} + \frac{\alpha_1 H}{\mu_2 t_1^2 t_2 G} \quad (A15)$$

$$N = \frac{\alpha M t_1 E(\eta)}{t_2 G(\eta)} + \frac{\alpha \sinh(t_1 \eta)}{t_1 t_2 G(\eta) \cosh(t_1)} - \frac{\alpha \sinh(t_2 \eta)}{t_2^2 G(\eta) \cosh(t_2)} - \frac{\alpha_1 M F(\eta)}{\mu_2 t_2 G(\eta)} - \frac{\alpha_1 \cosh(t_1 \eta)}{\mu_2 t_1^2 t_2 G(\eta) \cosh(t_1)} + \frac{\alpha_1}{\mu_2 t_1^2 t_2 G(\eta)}. \quad (A16)$$

For obtaining the value of  $P$ , we use Eq. (A17), which implies  $P = 2/R$ :

$$\int_{\eta}^1 u_1 dy + \int_{-1}^{\eta} u_2 dy = 2. \quad (A17)$$

where value of  $R$  is given by:

$$R = \frac{M}{t_1} [E(1) - E(\eta)] + \frac{N}{t_2} [G(\eta) - G(-1)] + \left[ \frac{\tanh(t_1)}{t_1^3} - \frac{\sinh(t_1 \eta)}{t_1^3 \cosh(t_1)} - \frac{1}{t_1^2} + \frac{\eta}{t_1^2} \right] + \left[ \frac{\alpha \sinh(t_2 \eta)}{t_2^3 \cosh(t_2)} + \frac{\alpha \tanh(t_2)}{t_2^3} - \frac{\alpha \eta}{t_2^2} - \frac{\alpha}{t_2^2} \right]. \quad (A18)$$

## Appendix B. Evaluation of Brinkman layer thickness near the interface

To obtain the thickness of the Brinkman layer near the interface, we utilize the relations as follows [3, 12, 34]:

$$u_1|_{y=\eta+\delta_1} = 1.01 u_{D_1}, \quad (B1)$$

$$u_2|_{y=\eta-\delta_2} = 1.01 u_{D_2}, \quad (B2)$$

where  $u_{D_1}$  and  $u_{D_2}$  denote the fluid velocity according to Darcy's law in porous regions above and below the interface of the channel, respectively.

On solving Eqs. (B1)-(B2), we get the expressions for Brinkman layer thickness, which are as follows:

$$\delta_1 = \frac{F(\eta)}{St_1} + \frac{1.01}{MSk_1^2 t_1} - \frac{1}{MSt_1^3} + \frac{\cosh(t_1 \eta)}{MSt_1^3 \cosh(t_1)}, \quad (B3)$$

$$\delta_2 = \frac{H(\eta)}{Tt_2} + \frac{1.01}{NTk_2^2 t_2} - \frac{\alpha}{NTt_2^3} + \frac{\alpha \cosh(t_2 \eta)}{NTt_2^3 \cosh(t_2)}, \quad (B4)$$

where  $S$  and  $T$  are defined as:

$$S = -\cosh(t_1 \eta) + \tanh(t_1) \sinh(t_1 \eta) - \frac{\sinh(t_1 \eta)}{Mt_1^2 \cosh(t_1)}, \quad (B5)$$

$$T = \cosh(t_2 \eta) + \tanh(t_2) \sinh(t_2 \eta) - \frac{\alpha \sinh(t_2 \eta)}{Nt_2^2 \cosh(t_2)}. \quad (B6)$$

## Appendix C. Boundary integral equation in terms of non-primitive variables

To obtain the boundary integral equation (BIE) corresponding to the obtained boundary value problem (BVP), it is necessary to first recall Green's second identity. Let us suppose, if  $f$  and  $g$  are two functions, which are the members of twice continuously differentiable classes over a domain (say)  $\Omega$ , then:

$$\int_{\Omega} (f \nabla^2 g - g \nabla^2 f) d\Omega = \int_{\Gamma} \left( f \frac{\partial g}{\partial n} - g \frac{\partial f}{\partial n} \right) d\Gamma \quad (C1)$$





where  $d\Gamma$  denotes an infinitesimal line or surface element depending on the dimension of the domain. To derive the BIE, corresponding to the BVP expressed in Eq. (24), we begin by substituting the functions  $f = \psi^{(i)}$  and  $g = G_i^L$ , into the above expression:

$$\int_{\Omega} (\psi^{(i)} \nabla^2 G_i^L - G_i^L \nabla^2 \psi^{(i)}) d\Omega = \int_{\Gamma} \left( \psi^{(i)} \frac{\partial G_i^L}{\partial n} - G_i^L \frac{\partial \psi^{(i)}}{\partial n} \right) d\Gamma \quad (C2)$$

By utilizing the relation between the vorticity variable and stream function, i.e.,  $\nabla^2 \psi^{(i)} = -\omega^{(i)}$ , above equation reduces into:

$$\psi(p)c(p) = \int_{\Gamma} \left( \psi^{(i)} \frac{\partial G_i^L}{\partial n} - G_i^L \frac{\partial \psi^{(i)}}{\partial n} \right) d\Gamma - \int_{\Omega} \omega^{(i)} G_i^L d\Omega \quad (C3)$$

where  $p$  is the field point,  $c(p)$  is called free term coefficient, and  $\nabla^2 G_i^L = \delta(r)$  is the singular Laplace equation. Subsequently, we substitute the functions  $f = \omega^{(i)}$  and  $g = G_i^C$  in Eq. (C1):

$$\int_{\Omega} (\omega^{(i)} \nabla^2 G_i^C - G_i^C \nabla^2 \omega^{(i)}) d\Omega = \int_{\Gamma} \left( \omega^{(i)} \frac{\partial G_i^C}{\partial n} - G_i^C \frac{\partial \omega^{(i)}}{\partial n} \right) d\Gamma \quad (C4)$$

On utilizing Eq. (7), above Equation reduces into:

$$\int_{\Omega} \omega^{(i)} (\nabla^2 - t_i^2) G_i^C d\Omega = \int_{\Gamma} \left( \omega^{(i)} \frac{\partial G_i^C}{\partial n} - G_i^C \frac{\partial \omega^{(i)}}{\partial n} \right) d\Gamma \quad (C5)$$

There is an inter-relation between the Laplacian operator  $G_i^L$  and the composite operator  $G_i^C$ , i.e.,  $(\nabla^2 - t_i^2) G_i^C = G_i^L$ , we substitute this relation in the above equation:


$$\int_{\Omega} \omega^{(i)} G_i^L d\Omega = \int_{\Gamma} \left( \omega^{(i)} \frac{\partial G_i^C}{\partial n} - G_i^C \frac{\partial \omega^{(i)}}{\partial n} \right) d\Gamma \quad (C6)$$


From Eqs. (C3) and (C6):


$$\psi(p)c(p) = \int_{\Gamma} \left( \psi^{(i)} \frac{\partial G_i^L}{\partial n} - G_i^L \frac{\partial \psi^{(i)}}{\partial n} \right) d\Gamma - \int_{\Gamma} \left( \omega^{(i)} \frac{\partial G_i^C}{\partial n} - G_i^C \frac{\partial \omega^{(i)}}{\partial n} \right) d\Gamma \quad (C7)$$

In this way, we can derive the BIE corresponding to the BVP using non-primitive variables.

## ORCID iD

Vishal Chhabra  <https://orcid.org/0009-0000-5612-0245>

Chandra Shekhar Nishad  <https://orcid.org/0000-0002-8941-4079>

Manoj Sahni  <https://orcid.org/0000-0001-7949-9147>



© 2023 Shahid Chamran University of Ahvaz, Ahvaz, Iran. This article is an open access article distributed under the terms and conditions of the Creative Commons Attribution-NonCommercial 4.0 International (CC BY-NC 4.0 license) (<http://creativecommons.org/licenses/by-nc/4.0/>).

**How to cite this article:** Chhabra V., Nishad C.S., Sahni M. Effect of Magnetic Field on Viscous Flow through Composite Porous Channel using Boundary Element Method, *J. Appl. Comput. Mech.*, 9(4), 2023, 1016–1035.  
<https://doi.org/10.22055/jacm.2023.43024.4006>

**Publisher's Note** Shahid Chamran University of Ahvaz remains neutral with regard to jurisdictional claims in published maps and institutional affiliations.

